Coordination Chemistry Reviews 469 (2022) 214669

Contents lists available at ScienceDirect

Coordination Chemistry Reviews

journal homepage: www.elsevier.com/locate/ccr

Review

Tailoring of electrocatalyst interactions at interfacial level to benchmark the oxygen reduction reaction

Ghulam Yasin [a,b,*], Sehrish Ibrahim [b], Saira Ajmal [a,*], Shumaila Ibraheem [a,*], Sajjad Ali [c,*], Ashok Kumar Nadda [d], Guoxin Zhang [e], Jasvinder Kaur [f], T. Maiyalagan [g], Ram K. Gupta [h], Anuj Kumar [i,*]

[a] Institute for Advanced Study, Shenzhen University, Shenzhen 518060, Guangdong, China
[b] State Key Laboratory of Chemical Resource Engineering, Beijing University of Chemical Technology, Beijing 100029, China
[c] Yangtze Delta Region Institute (Huzhou), University of Electronic Science and Technology of China, Huzhou 313001, China
[d] Department of Biotechnology and Bioinformatics, Jaypee University of Information Technology, Waknaghat, Solan 173 234, India
[e] Department of Electrical Engineering and Automation, Shandong University of Science and Technology, Qingdao, Shandong 266590, China
[f] Department of Chemistry, Gurukula Kangri University, Haridwar, India
[g] Electrochemical Energy Laboratory, Department of Chemistry, SRM Institute of Science and Technology, Kattankulathur 603203, Tamilnadu, India
[h] Department of Chemistry, Kansas Polymer Research Center, Pittsburg State University, Pittsburg KS-66762, USA
[i] Nano-Technology Research Laboratory, Department of Chemistry, GLA University, Mathura, Uttar Pradesh 281406, India

ARTICLE INFO

Article history:
Received 7 February 2022
Accepted 7 June 2022

Keywords:
Electrocatalysts
Oxygen reduction reaction
Interface
Active sites
Interfacial engineering

ABSTRACT

The cathode process, oxygen reduction reaction (ORR), is crucial for producing green and reliable energy from the reorganization of chemical bonds in fuel cells. However, the application of ORR is limited due to its inefficiency, which can not only be attributed to the linearity of ORR intermediates binding energies (E_b^{*OOH}, E_b^{*O}, E_b^{*OH}) on the catalyst's active site (represented as *) but also to the serious influences of the watery environment on active sites. In an aqueous environment, catalyst interactions, including covalent, ionic, and van der Waals forces, at the interfacial level are critical in determining the catalytic activity and can considerably alter the kinetics and selectivity of ORR. Therefore, the interfacial confinement's unique properties can provide exciting new possibilities for designing molecular as well as material-based catalysts for ORR. Although several published reviews have focused on developments in interfacial engineering for electrocatalysis, not specifically for ORR, this domain still lacks an inclusive debate on the mechanism of interface structures during ORR. We highlighted the most recent employed strategies for interface structure construction and the role of interfacial interactions during ORR. Finally, the barriers and prospects for the construction of electrocatalysts based on such concepts as control of interfacial interactions, engineering, and technologies are also discussed.

Contents

* Corresponding authors.
E-mail addresses: yasin.bzu@hotmail.com, yasin@mail.buct.edu.cn (G. Yasin), sairaajmal6@outlook.com (S. Ajmal), shumaaila01@outlook.com (S. Ibraheem), sajjad@alum.imr.ac.cn (S. Ali), anuj.kumar@gla.ac.in (A. Kumar).

https://doi.org/10.1016/j.ccr.2022.214669
0010-8545/

1. Introduction

1.1. Inspirations

Energy generated by the re-organization of chemical bonds may be considered a never-ending source of renewable energy. Fuel cells (FCs) function on the above principle, following the transformation of chemical bonds' energy directly into electrical energy. The cathode process in FCs, oxygen reduction reaction (ORR), is a fundamental electrocatalytic mechanism that involves the electronic communication between dioxygen (O_2), and protons (H^+) to form water (H_2O) as a by-product [1]. However, ORR is difficult to accomplish quickly at a practical level without a suitable electrocatalyst. A wide range of catalysts have been reported in this context, but due to the presence of a typical watery environment and the involvement of nH+/e– transfer steps, forming the *OOH, *O, and *OH intermediates, on the catalyst surface, only a few of them, including noble metals and molecular-based catalysts, can cause ORR to proceed quickly with non-remarkable overpotentials [2–4,5]. Although the compositional, as well as structural alterations in these catalysts significantly improved the catalytic activity, the further enhancement in their catalytic performance by controlling the interfacial interactions is very essential for the development of FCs. Therefore, the hunt for innovative and robust electrocatalysts with well-defined interfacial engineering continues to be a major focus of research and development in this field.

1.2. Fundamentals of interfacial effects on electrocatalytic reactions

In the previous decades, many attempts have been made to design efficient catalysts for ORR by adjusting the adsorption strength and surface binding energy of the catalysts using various approaches. Among these approaches, few are (i) tailoring the catalyst's composition: it has been demonstrated that catalysts composed of two or more metallic components show significant electrocatalytic activity when compared to catalysts containing only a single metallic component. The improved catalytic activity could be attributed to the typical electronic as well as synergistic influences between the different metallic components [6], (ii) controlling the catalyst's architecture and size: the catalyst architecture with an appropriate shape and size may increase the exposure of active sites that are accessible for the catalysis [7], (iii) tailoring of inherent activity of electrocatalysts via surface structure engineering [8], and (iv) using catalyst support that might increase active sites per unit area, conductivity, and porosity to boost the catalyst's performance [9].

Aside from the aforementioned strategies, it is also believed that catalyst interactions at the interfacial level can exhibit a variety of characteristics, such as active site stabilization as well as changes in their electronic structures, easy electron transfer, and optimal binding energies of reaction intermediates, thereby improving their overall electrocatalytic performance [10,11]. Here, a logical comparison between an interface and a surface needs to be introduced. An interface or surface, in a broader sense, is a barrier between two phases, and the terms are frequently used interchangeably. When a macroscopic entity (the interior) comes into contact with its own surroundings, it is referred to as a "surface". However, a thin 3D layer separating the two phases in contact is referred to as an "interface" instead of a "surface" in some contexts. The idea of interfacial interactions has expanded significantly in the last few years, although our understanding is still at an early stage [8,12]. A fundamental graphical representation of an interface between two components along with a facile H^+/e– transfer pathway is shown in Fig. 1a and the modes of action during electrocatalytic reaction on the interface are shown in Fig. 1b. The electron transfer is enabled by the interface between both the electrocatalyst's components, and the reaction rate is influenced by the binding energy between the reactant molecules and components. Consequently, it is possible to accomplish effective electrocatalysis by adjusting the adsorption and desorption strengths between active sites and reactant molecules by altering the surface of the catalyst. The entire electrocatalytic process consists of three steps: (i) chemisorption of reactant molecules on the electrocatalyst's surface or interface, (ii) excitation of these molecules, forming intermediates, and (iii) the detachment of product molecules from the catalyst surface. Therefore, the binding energy between reaction intermediates and the active sites is one of the important factors that affect the overall performance of a electrocatalytic reaction, and it should be neither too strong nor too weak, as also suggested by the Sabatier principle. However, there is no widely acknowledged logical scientific justification for these approaches correlating the interfacial interactions, so a great deal of research is going on in order to establish universal activity descriptors for electrocatalytic reactions.

The thermodynamic, as well as kinetic correlations among the ORR intermediates, have been studied to establish the universal activity descriptors for both homogeneous and heterogeneous catalysts. Therefore, ORR efficiency may be improved by ensuring that its kinetics under the electrolytic medium is properly controlled by monitoring H^+ activity at the interfacial electrode–electrolyte contact [13]. However, H^+ activity monitoring at the atomic level during ORR is troublesome due to the presence of a watery medium, where multiple interactions are involved, making it challenging to figure out the exact process. The interfacial interactions of hybrid materials with customized interfaces regulating H^+ activity to greatly increase ORR performance were revealed very recently [14–16]. Interface structures with the potential benefit of transferring electrons or intermediates between components are often

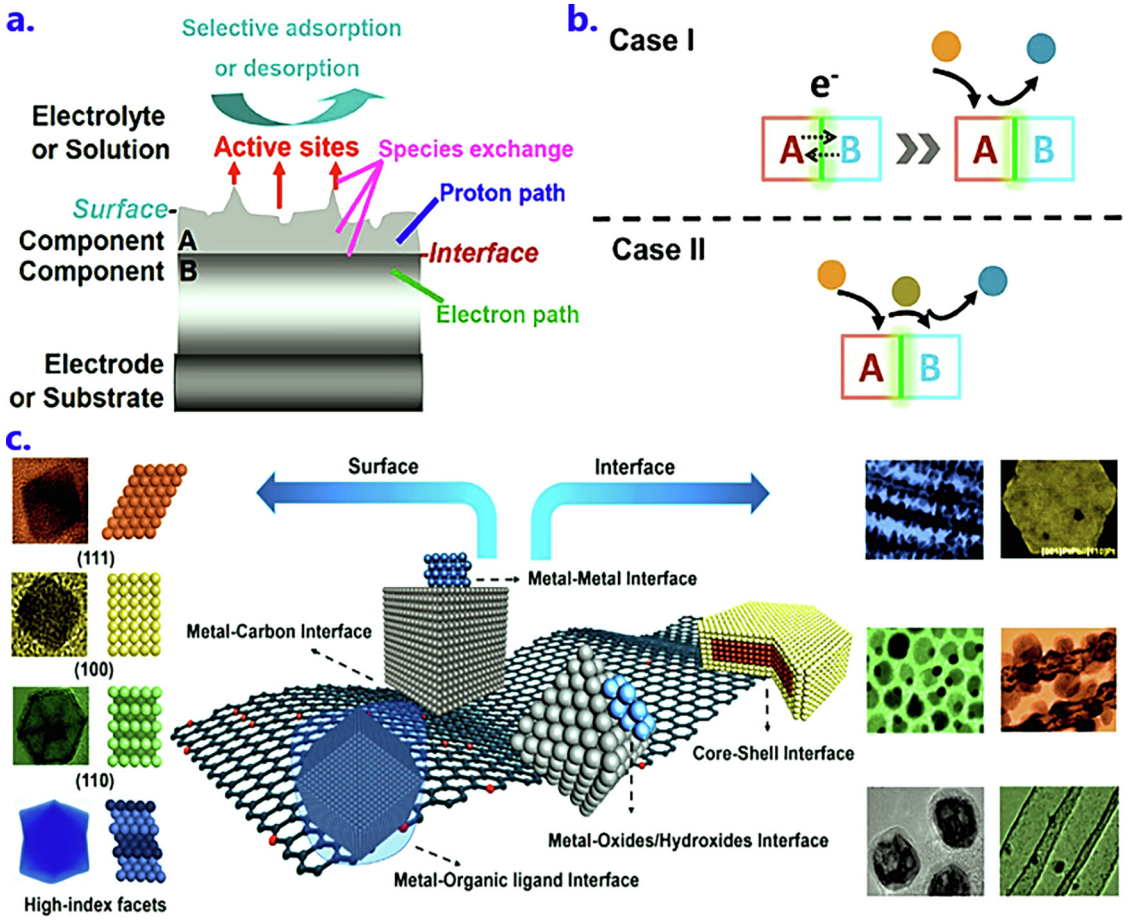

Fig. 1. a. A schematic representation of an ideal triple-phase (TP) boundary with e−/H+ paths, and solution phase coexisting with active sites. Taken from [22], copyright 2015, Elsevier publishing group. b. A catalyst that consists of two components A and B connected via an interface. Component A offers the catalytic active sites in an instance (case I). Component B optimizes A's electrocatalysis by modifying its surface environment. For instance (case II), adsorption and desorption take place independently on A and B. Taken from [23], copyright 2019, Wiley-VCH publishing group. c. Electrocatalysis Nanocrystal Surface and Interface Engineering Research Efforts are outlined in a diagram. Taken from [1], copyrights 2018, Elsevier publishing group.

used to link two or more distinct components [17,18]. Rational control of interface atomic arrangement is responsible for monitoring physicochemical characteristics of electrocatalysts, including electrocatalytic performance [19–21]. Furthermore, by altering strain, ligand effect, and surface orientations, the intrinsic activity of ORR has been greatly enhanced. The typical outlined nanocrystal surface and interface engineering research activities of the relevant scientific community are depicted in Fig. 1c.

Aside from interface engineering, the choice of electrolytes and ionic liquids might open up new possibilities for non-covalent interactions to control H^+ activity. For instance, the inclusion of an ionic liquid layer between the Au and Pt surfaces caused a chemical feedstock that restricted the H^+ activity, thereby enhancing ORR dynamics. Thus, a wide range of ionic liquids may be employed to modulate H^+ activity and H^+ transfer barriers, allowing ORR tunability at a practical level in the near future. These approaches can provide essential insights into the mechanisms of H^+ transport at the quantum level, and therefore, the scientific community may be able to better realize the interactions between hydrogen ions and electrons on catalytic surfaces [24].

Previously, only a few review articles focused on the interface structure of the diverse electrocatalytic reactions [25]. The aim of this study is to present a brief overview of the interfacial interactions and the most recently developed interfacial engineering for the electrocatalytic ORR. For a better understanding, the adsorption-energy scaling equations for ORR and their origins have also been highlighted. Furthermore, the strategies that are expected to overcome the scaling relations during the ORR process are discussed in detail, including the role of hydrophobic ionic liquids, control of H^+ activity using ionic liquid layers, hydrophobic cations, strain effects, changing the solvent composition, and functional groups/H^+-relay groups at the interfaces. Finally, the issues and the prospects with the interfacial forces and engineering for ORR are also discussed in the concluding section.

2. Fundamentals of electrocatalytic ORR

2.1. Electrocatalytic ORR

Based on O_2-adsorption orientation as well as O-O link rupture energy barriers on the active site, ORR proceeds following two different routes in acidic (Eq. (1) – Eq. (3)) as well as alkaline (Eq. (4) – Eq. (6)) media; 4e− ORR (O_2 converts into H_2O) or 2e− ORR (O_2 converts into H_2O_2) (Fig. 2a). The 4e− ORR involves O–O bond dissociation, liberating maximum free energy, whereas 2e− ORR releases almost its half of the free energy due to the release of high O–O bond dissociation energy. The 2e− ORR process generates reaction intermediates (H_2O_2) capable to block the active sites at the catalyst surface, as well as the destruction of the catalyst surface due to oxidation of the carbon framework, thus, drastically reducing the ORR performance. Therefore, the catalyst-assisted reduction of O_2 to H_2O through the $4e^-$ the pathway is favorable to achieve the high efficiency of ORR.

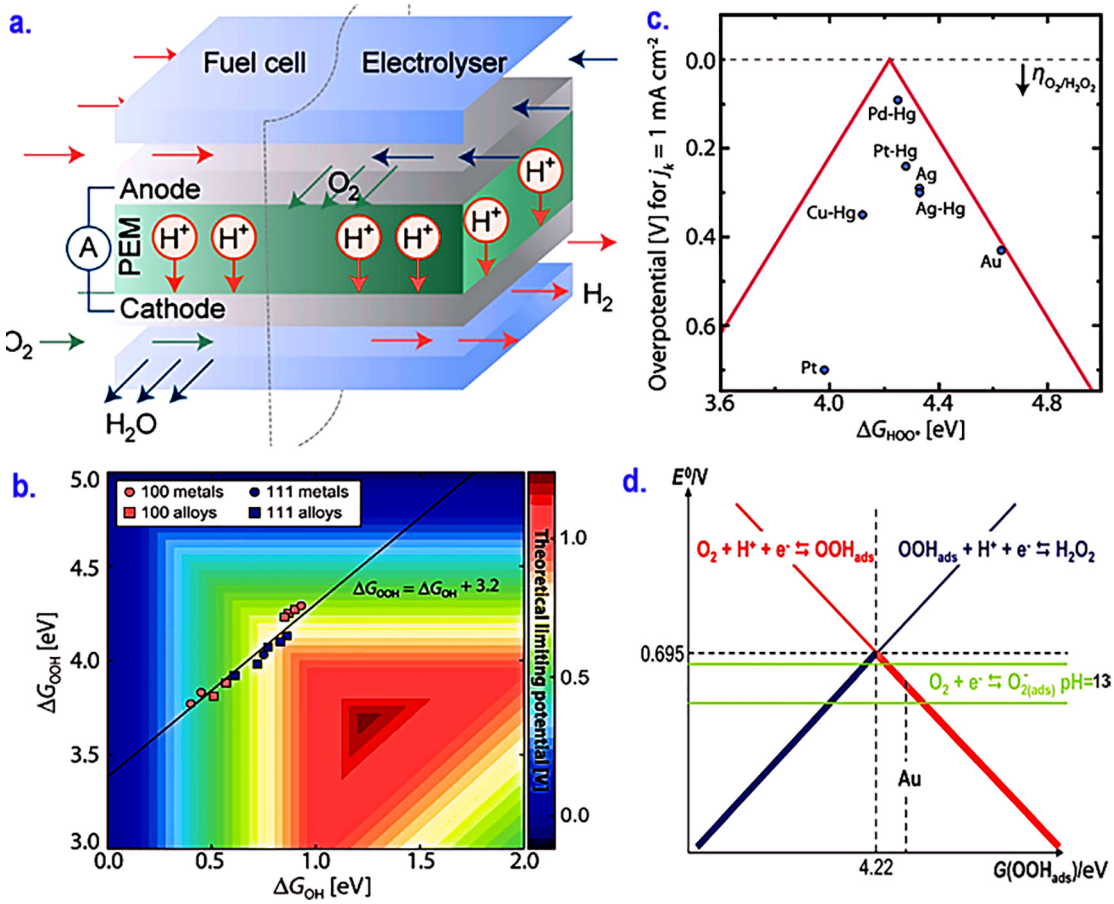

Fig. 2. a. The operating concept for a typical FC [32], b. A systematic representation for the $\Delta G^{*OOH} = \Delta G^{*OH} + 3.2 \pm 0.2$ eV relationship for ORR intermediates, c. The 4e− ORR volcano plot for various metal facets. Taken from [33], copyright 2017, American Association for the Advancement of Science (AAAS) publishing group. d. The 2e− ORR volcano plot. Taken from [13], copyright 2013, Royal Society of Chemistry (RSC) publishing group.

ORR in an acidic aqueous environment:

$$O_2 + 4H^+ + 4e^- \rightarrow H_2O\ 1.229\ \text{V vs SHE (at pH} = 0) \quad (1)$$

$$O_2 + 2H^+ + 2e^- \rightarrow H_2O_2\ 0.695\ \text{V vs SHE} \quad (2)$$

$$H_2O_2 + 2H^+ + 2e^- \rightarrow 2H_2O\ 1.77\ \text{V vs SHE} \quad (3)$$

ORR in an alkaline aqueous environment:

$$O_2 + H_2O + 4e^- \rightarrow 4OH^-\ 0.401\ \text{V vs SHE} \quad (4)$$

$$O_2 + H_2O + 2e^- \rightarrow HO_2^- + OH^-\ -0.065\ \text{V vs SHE} \quad (5)$$

$$HO_2^- + H_2O + 2e^- \rightarrow 3OH^-\ 0.867\ \text{V vs SHE} \quad (6)$$

2.2. ORR scaling relations

The O_2-adsorption on a single metal site may take place via (i) side-on O_2-adsorption onto the active site; it involves e− donation from O_2-2p (π) orbitals into empty dz^2 (3d) orbital of the metal site along with back bonding from t_{2g} orbitals of metal into the $2p^*$ (π^*) orbitals of O_2, (ii) bridged O_2-adsorption on two metal sites; in this case, O_2-adsorption is facilitated by the dissociative nature of the O–O link being broken by s-interaction and (π)-back bonding between O_2 and metal sites [26,27]. If both O-atoms connect to two metal sites individually, the 4e− ORR can be easily happened due to restriction for the H_2O_2 formation as an intermediary on the catalyst surface (Eq. (7), 8, and 9 for the 4e− ORR via a dissociative mechanism, whereas, Eq. (10), 11, 12, 13, and 14 for the 2e− ORR followed by associative mechanism, in an acidic environment) [28], and (iii) the end-on adsorption; although it includes the transfer of e-density into a metal's dz^2 orbital from the hybrid orbital of oxygen, it is not capable of forming an O-O bond by the dissociative process, and so favors selective 2e− ORR (Eq. (4), 5, and 6) [29].

Dissociative pathway:

$$O_2 + * + * \rightarrow *O + *O \quad (7)$$

$$*O + *O + 2H^+ + 2e- \rightarrow *OH + *OH \quad (8)$$

$$*OH + *OH + 2H^+ + 2e- \rightarrow 2H_2O + * + * \quad (9)$$

Associative pathway:

$$O_2 + * \rightarrow *2O_2 \quad (10)$$

$$*O_2 + H^+ + e- \rightarrow *OOH \quad (11)$$

$$*OOH + H^+ + e- \rightarrow H_2O_2 \quad (12)$$

$$*OOH + H^+ + e- \rightarrow *O + H_2O \quad (13)$$

$$*O + H^+ + e- \rightarrow *OH \quad (14)$$

$$*OH + H^+ + e- \rightarrow * + H_2O \quad (15)$$

For the associative pathway, it is theoretically possible to identify a catalyst having a non-remarkable overpotential with optimum ΔG_{*OOH} (Fig. 2b). When designing effective catalysts, it is crucial to understand how to regulate the binding energies of

intermediates E_b^{*OOH}, E_b^{*OH}, and E_b^{*O} on active sites. The universal scaling relation, $\Delta G^{*OOH} = \Delta G^{*OH} + 3.2 \pm 0.2eV$, between the intermediates, is true for the majority of electrocatalysts, including metal alloys and metal-nitrogen-carbon (M-N-C) materials (Fig. 2c)[30,31]. This scaling relation imposes an activity constraint, requiring a theoretical overpotential of 0.3–0.4 V for the electrocatalysts, even if they have optimum adsorption strength. This conclusion is also supported by the experimentally defined ORR overpotential trend for a variety of electrocatalysts, including the Pt-based materials.

2.3. Origin of scaling relations for ORR

All ORR intermediates attach to the active site by atomic oxygen in accordance with the linear relationship, and various active sites have been explored to describe the scaling relation between *OOH (1) and *OH (2) intermediates (Eq. (16)).

$$\Delta G_2 = A_{1,2}\Delta G_1 + B_{1,2} \quad (16)$$

The e− counting rule, like the octet rule, determines the slope $A_{1,2}$ and the e− counting, as well as the nearest neighbor counting rules, define the intercept $B_{1,2}$. As a result, the scaling relationship slope for *OH (*OOH) and *O is roughly 0.5 [34 35,36]. It can be attributed to the requirement of one or two electrons on the O atom of these intermediates in the octet rule. Scaling up from *OOH to *OH has a slope of roughly 1.0 due to the octet rule requiring one electron for each. An approach is to use the electron-counting procedure to calculate the intercept $B_{1,2}$ and its slope, which is linearly proportional to the coordination number (Fig. 2d).

Therefore, these scaling relationships between ORR intermediates can be viewed as expressions of the aforementioned *O features. An intriguing discovery is that the scaling relationship between the intermediates may have a constant intercept as the slope approaches 1.0. For example, the low-index metals and their alloy surfaces [30,37] have intercepts of 3.2 ± 0.2 eV for the *OOH and *OH intermediates. However, it is also true that this intercept is independent of the ORR intermediates adsorbing onto the catalyst surfaces, having the identical coordination structure, irrespective of their valences.

According to the linear scaling of adsorption-free energies, there is less room for optimization and the creation of catalytic sites than adsorbed intermediates. As a result, several descriptors, including the ΔG^{*O}-ΔG^{*OH} relationship [38], d-/p-bands centers [39,40], e.g. occupancy [41,42], the (generalized) coordination number [34,43], the metal–oxygen covalency [44,45], and the surface distortion [46], are being developed to minimize the ORR overpotential in volcano curve. This scaling relationship has an intriguing side effect in that it limits the construction of catalysts since their activity cannot be enhanced farther beyond the activity volcano curve. Therefore, a classical shift in the design of ORR electrocatalysts is necessary to overcome or avoid this scaling rule. In this regard, strategies based on the control of multi-steps H^+/e− transfer processes could be considered as a conceptual route for the development of the ORR process.

2.4. Decoupled n(H^+/e-) transfer mechanisms for ORR

Typically, the equations from 5 to 9 may be used to quantify ΔG-scaling relationships between the ORR intermediates, because these equations are valid between them. In practice, the scale with RHE thermodynamically shows an onset shift of 60 mV per pH, even though it does not vary with pH with the NHE scale. Due to the involvement of decoupled H^+/e− transfer routes, a charged intermediate is produced in this event. When charged intermediates are included, the adsorption energy scaling relationship, having an intercept of 3.2 eV, is not broken for the *OOH and *OH reaction intermediates [47]. When O_2 is poorly bound at the active site (right side of volcano curve), ORR can follow two contending pathways, producing *OOH and $*O_2$− species, followed by the decoupled H^+/e− transfer route, which is further advantageous at higher pH thermodynamically[13]. In contrast, the volcano curve's left side follows a 4e− transfer pathway with strong O_2 binding on active sites. Due to these facts, the pH of the electrolytes affects the onset potential of the catalysts, thereby, influencing the overall catalytic activity.

3. Strategies to benchmark the ORR performance tailoring interfacial interactions

ORR catalysts must be overpotential-free, which means that they must have the ideal energy difference, ΔG_{*OOH}-ΔG_{*O}, of 2.46 eV for the *OOH and *O intermediates, as well as low barriers for nH^+/e− processes. Therefore, apart from the design of electrocatalysts, and optimizing their surfaces and electronic structures, tailoring of their H^+ activity via interfacial strategies can also break the linear scaling of ORR intermediates [48]. Usually, a catalyst's surface or interface is a good spot to accomplish any electrochemical reaction involving multiple electron transfers and intermediates. When it comes to the chemistry of a catalytic reaction, the atomic and electronic structures of the catalyst's surface or interfaces, as well as interfacial interactions, are critical factors. For instance, interfacial engineering is reported to be responsible for the synergistic effects on H^+/e− transfer and the movement of intermediates. Moreover, due to interfacial engineering, electrons may be redistributed to facilitate charge transfer between the catalyst and chemical intermediate at the interface [1,49]. In this section, the facile strategies for tailoring of electrocatalyst interfacial interactions that might improve electrocatalytic ORR performance, and the theoretical insights have been discussed in detail.

3.1. Creating the interfacial bonds

Interfacial bonds can often be exposed to control the redistribution of electrons in hetero-interfaces and to induce the e− transfer from active sites to substrates during electrocatalysis. Therefore, this approach can be used to modify the electronic properties of the interface components, and thereby, improving the ability and chemical stability of active sites during the chemisorption of ORR intermediates [50,51]. For instance, Xinliang Feng et al. [52] fabricated a 2D black phosphorus (BP) linked with graphitic carbon nitride (BP-CN-c) material as an efficient and eco-friendly ORR electrocatalyst. Fig. 3a illustrated the BP-CN-c material's systematic synthesis strategy as well as a graphical depiction of the electron transfer from BP to graphitic carbon nitride. Fig. 3(b-c) shows the morphology of graphitic carbon nitride and BP-CN-c material, clearly demonstrating the interaction between CN and BP. The DFT calculation suggested that the covalent interaction between BP and CN-c was mainly responsible for the improved electrocatalytic efficiency of this catalyst. They suggested that the polarized covalent bond between both the P and N in this catalyst may effectively control the e− transport from BP (donor) to CN-c (acceptor), thereby improving the binding strength of the ORR intermediates on phosphorus atoms. As a result, the BP-CN-c catalyst demonstrated superior ORR activity (Fig. 3(d-e)). Because of this new understanding of interfacial covalent bonding, this work opens the door to designing low-cost, robust, and novel metal-free catalysts for electrocatalytic reactions.

In another work, Mukherjee and colleagues developed an efficient catalyst, $Pt/NbO_x/C$, and investigated the effects of metal and metal oxide interactions on its ORR activity, employing an

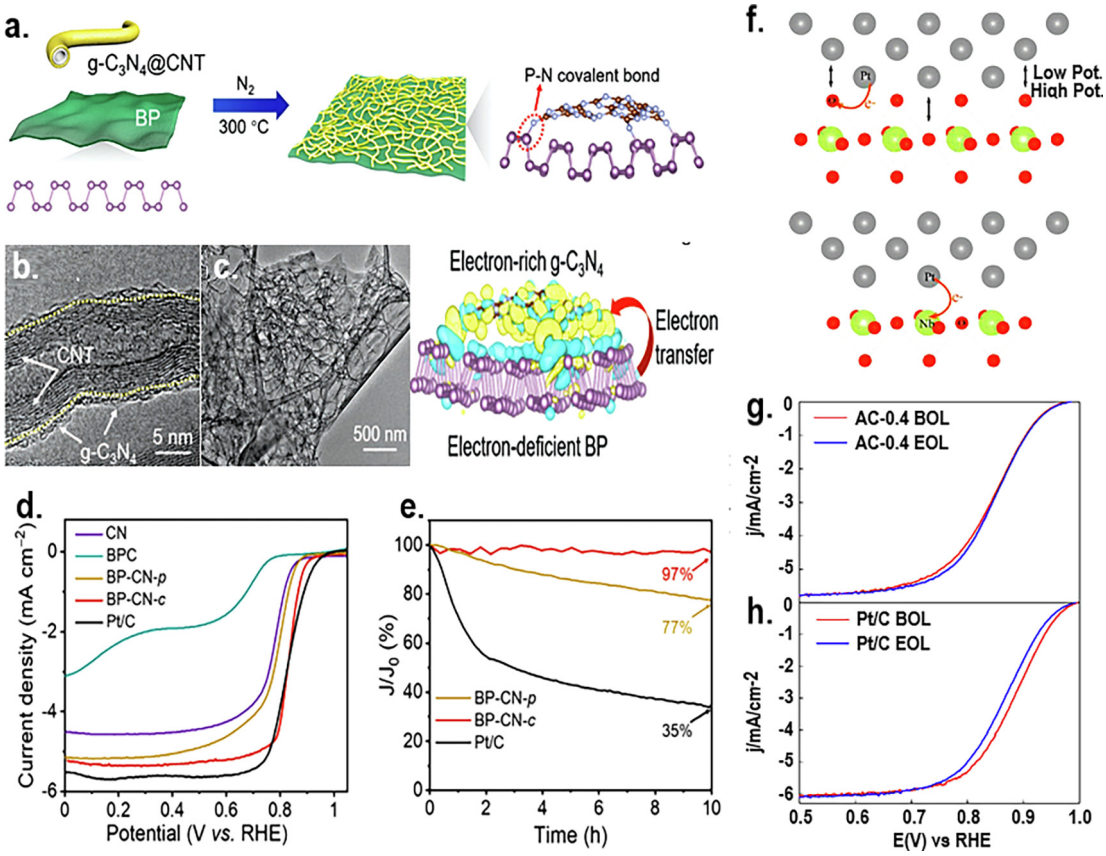

Fig. 3. a. The systematic diagram of BP-CN-c materials, The TEM pictures of b. CN, c. BP-CN-c along with the e− transfer path between BP and CN-c, d. LSVs for the counter samples and BP-CN-c catalyst, recorded at 5 mV/s with 1600 rpm, e. CA plots recorded at counter samples and BP-CN-p at 0.7 V. Taken from [52], copyrights 2021, Wiley-VCH publishing group. f. Charge transfer at the interface of Pt with saturated Nb_2O_5 and Pt with unsaturated NbOx. LSVs for g. AC-0.4 h. Pt/C at BOL and EOL stages. Taken from [53], copyrights 2017, ACS publishing group.

electrocatalyst as the model system [53]. The results indicated that the interfacial bonds between Pt and O (Pt-O) were formed during the penetration of O from the Pt-clusters, followed by association with Nb, as seen in Fig. 3f. The strong Pt-O electronic coupling, via facile e− transfer between the NbOx and Pt, controlled the Pt's electronic structure, thereby improving the ORR activity (Fig. 3(g-h)). This study can be considered as a strong commitment to electronic alteration at the interface between the catalyst's surface and conductive support via interfacial interactions can significantly boost the ORR performance [54–56].

3.2. Creating the strain effects

Solid materials deform in a variety of ways, and one of the most important ways is strain, which is based on physics concepts. When the lattice parameters of distinct components aren't aligned, the strain effect occurs, and it gets weaker as it moves from the interface to the surface of the hybrid material in question [57 58]. Lattice distortion may be used to measure the length change in atomic bonds generated by strain. The stability and activity of an electrocatalyst are affected by the internal strain effects that impact its surface electronic structure and binding energy toward an adsorbate. Therefore, the activity and stability of the catalysts can be improved by designing the microstrain or localized lattice strain in a logical way [59,60].

In addition, a change in strain in alloy-type materials might cause the alteration in the d-band center of transition metal. For example, the band narrowing caused by compressive strain favors the down-shift in the d-band center to maintain the d-band electron filling [61], resulting in the increase in oxygen binding energy, and vice versa for band narrowing caused by tension. Therefore, this idea can be used to break the scaling relationships of ORR intermediates to achieve superior ORR activity of the electrocatalysts. It is the same process that causes the d-band center to move higher for late transition metals [62–64]. For instance, to boost the ORR performance of the Pd-Au alloy, Zhu et al. [65] altered its d-band center by creating the local strain (mismatch in lattice parameters) at the interface of graphene oxide supported Pd-Au alloy, as illustrated in Fig. 4a. The mismatch in lattice parameters between the Pd and the Au is evident in the HR-TEM (Fig. 4b), which shows that the epitaxial layers of Pd at the Pd-Au interface are responsible for the creation of tensile stress, while the compressive stress is due to the Au components. The LSV investigations revealed Pd-Au alloy to possess excellent ORR activity (Fig. 4c). The theoretical calculations for the interfacial Pd sites at + 5% tensile stress revealed that the binding energy of *O got reduced while the binding energy of *OH got increased (Fig. 4d). Due to these facts, the cause in a reduction in rate-determination step energy ($O^* + H_2O + e- = OH^* + OH^-$) improved the ORR activity of this material has also been supported by the LSV investigation on Pd-Au alloy.

In a recent study, Khorshidi et al. [66] found that strain may influence the binding energy and scaling relationships between ORR intermediates when the catalyst's structure is altered to become selectively coherent with a particular intermediate. In another work reported on N-doped graphene, Xie et al. used DFT simulations to examine the influence of several deformations (electronic and compositional) on the binding strengths of ORR intermediates. They demonstrated that the adsorption of *O was

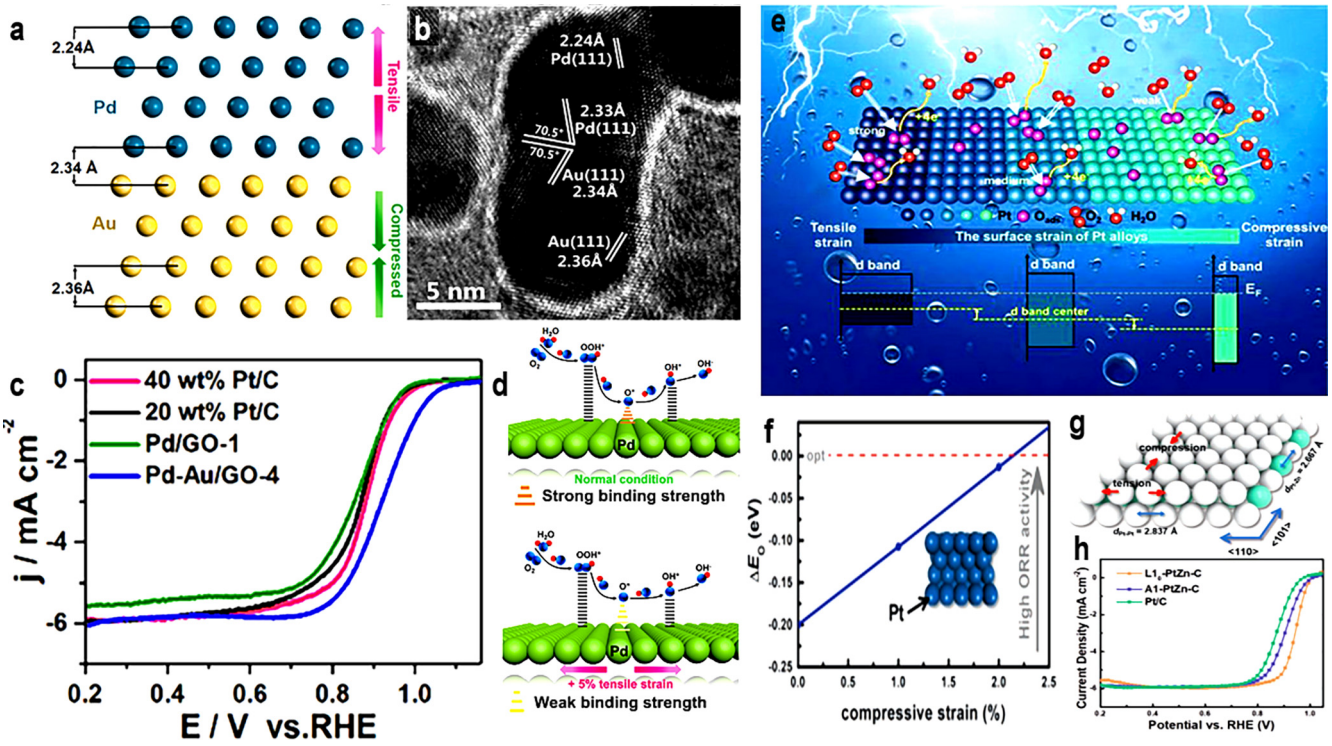

Fig. 4. a. The lattice representation of Pd-Au material, and b. HR-TEM pictures of Pd-Au material's lattices, c. LSVs Pt/C, Pd/GO-1, and Pd-Au/GO-4 catalysts, d. the schematic ORR mechanism ORR on Pd-Au catalyst, having tensile strain (+5%). Taken from [65], copyrights, 2020, Elsevier publishing group. e. the drawing of d-band center vs surface strain for Pt/C catalyst. Taken from [67], copyrights 2021, IOP publishing group. e. illustration for the mismatch of L1 0 –PtZn (A) and A1-Pt lattices, f. strain dispersal on (1 1 1) surface of A-lattice, g. standard atomic organization for A. Taken from, copyrights 2020, WILEY-VCH publishing group.

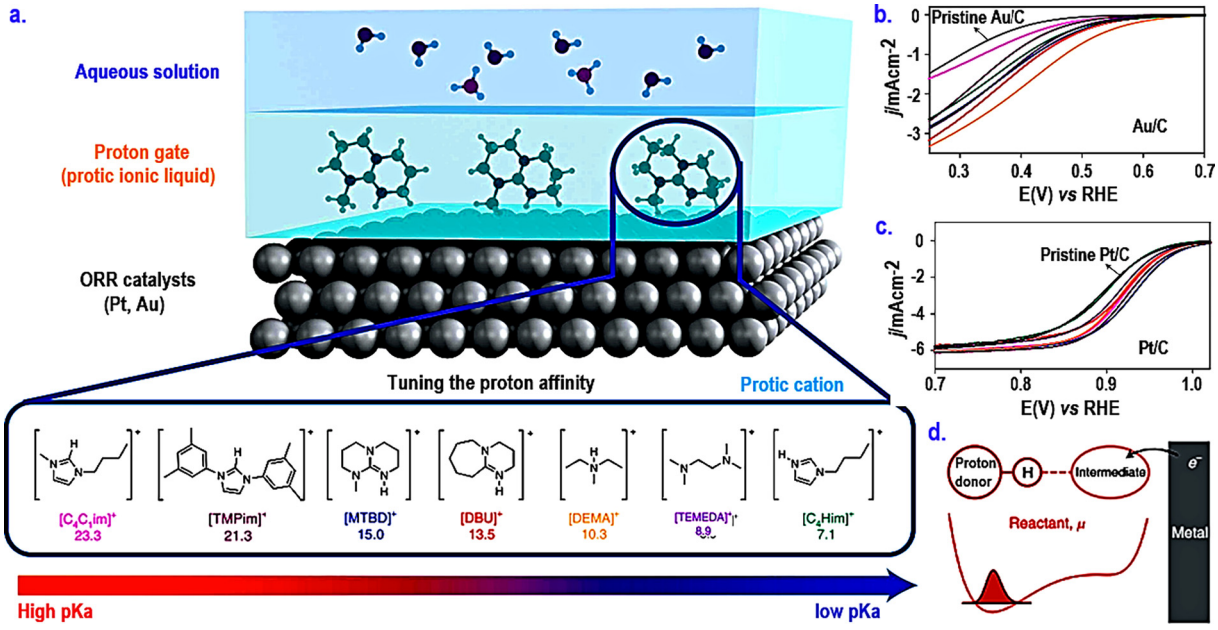

Fig. 5. a. Local proton concentrations can be tuned for optimal ORR. ILs, which have pKa values ranging from 7.7 to 23.3, modify the local H^+ activity for ORR on the metallic catalyst's surface. ILs-modified ORR, measurements of Au/C and Pt/C acidic environment b. Au/C, and c. Pt/C. d. on H^+-bonded contact, the PCET scheme. Reproduced with permission [69]. Copyrights 2021, Nature publishing group.

found to be improved by tensile strain, but the adsorption of *OH and *OOH was shown to be unaffected. The tensile tension and *O-adsorption tend to rupture the C–N bond in this manner. However, the scaling relationship between *O, *OH, and *OOH cannot be broken by the local curvature. There will need to be more studies on other catalyst surfaces in the future to support this claim.

Comparing the ordered Pt alloys, Yuchen Qin et al. [67] demonstrated improved catalytic activity and stability with disordered Pt alloys as illustrated in the graphical abstract (Fig. 4e). This was attributed to the higher structural stability of ordered Pt alloys. It was possible to preserve the ordered structure even after ORR testing, with just the appearance of Pt-like skin appearing on only a

few surfaces at atomic levels. Theoretical simulations show that ordered Pt alloys have better ORR performance than disordered alloys because of the stronger Pt–metal covalent connection and the larger negative heat of formation. Making thin-film structures out of platinum alloy catalysts is another significant advancement in this field. Carbon erosion, contact resistance between NCs and carbon, and the fraction of low-coordination-number atoms may all be reduced by spreading Pt alloy nanocrystals on a nanostructured polymer thin film. Compared to thin-film structures, there is a considerable difference in the ORR activity of Pt alloy catalysts.

Liang et al., [68] synthesized L10-PtZn intermetallic nanoparticles (NPs) with approximately a 4 nm diameter for use in PEMFCs as the catalyst to improve the ORR performance. These NPs displayed superior activity with a power density of 2.00 Wcm^{-2} and excellent durability (only 16.6 % mass activity losses after 30,000 CV cycles). According to DFT calculations, the surface Pt-Pt distances in PtZn NPs are modulated by biaxial stresses that arise during the disorder–order transition (Fig. 4f), and the Pt-O binding (Fig. 4g) is optimized for ORR activity enhancement (as supported by LSV studies (Fig. 4h)) by the higher vacancy formation barrier of Zn atoms in an ordered structure.

3.3. Controlling the H^+ activity using ionic liquids

Despite the fact that better ORR activity may be linked to improved hydrophobicity at Pt-ionic liquids (ILs) interfaces as well as higher O_2 solubility in ILs, it is unclear how to develop materials to regulate ORR activity in a cost-effective manner using the above-described strategies. Recently, the ORR activity of Pt/Au material was reported with significant improvement, which was attributed to the interfacial H^+-activity of ILs. In acid media, a wide variety of protic ILs could be exposed in the interfacial layer, altering the ORR dynamics of Pt/Au materials (Fig. 5a). Protic cations are thought to work as H^+-relays at the interface between these transition metals and bulk electrolytes. In ILs [69], it is feasible to measure the H^+-activity that influences the ORR kinetics. Cations with different pKa values ($[C_4C_1im]^+$ pKa = 23.3; $[TMPim]^+$ pKa = 21.3; $[MTBD]^+$ pKa = 15.0; $[DBU]^+$ pKa = 13.5; [DEMA].) were used to influence the activity of Au and Pt, displaying the 2e− ORR and 4e− ORR, respectively[70–72]. For Pt and Au, protic cations have been proven in the past to boost their ORR activity, because protic cations tend to form a strong hydrogen bond with the rate-limiting ORR intermediate, reducing the energy barrier.

The prediction of PCET kinetics based on H^+ vibrational wave functions at the H-bonding interface led to the rise of ORR exchange current density, which was verified by the observation of faster H^+ tunneling kinetics. To modulate local H+-activity for ORR, ILs coatings were applied to Au/C and Pt/C surfaces. The ORR activity was evaluated using RDE measurements for Au/C (6.01%) and Pt/C (19 wt%), as shown in Fig. 5b,c, respectively. The ILs layers containing protic cations on the interface of Au and Pt were revealed to be 1 nm thick. Before electron transfer, an H^+ donor atom possessed a low H^+ potential, and the ORR intermediate accepted electron from the electrode surface and decreased this potential, allowing H^+ transfer from the ORR product, as shown in Fig. 5d. Researchers will be able to better understand PCET, which is a type of PCET that uses electrochemical reactions. This opens the door to new ways to improve the electrocatalytic activity of not only O_2, but also CO_2, N_2, and other electrochemical reactions, by changing the local H^+-activity near the active sites and the interfacial hydrogen-bond strength.

3.4. Introducing the hydrophobic ionic liquids/cations

Catalytic material composition and structural tuning alone may not be enough to fulfill the demands of real-world devices, neces-

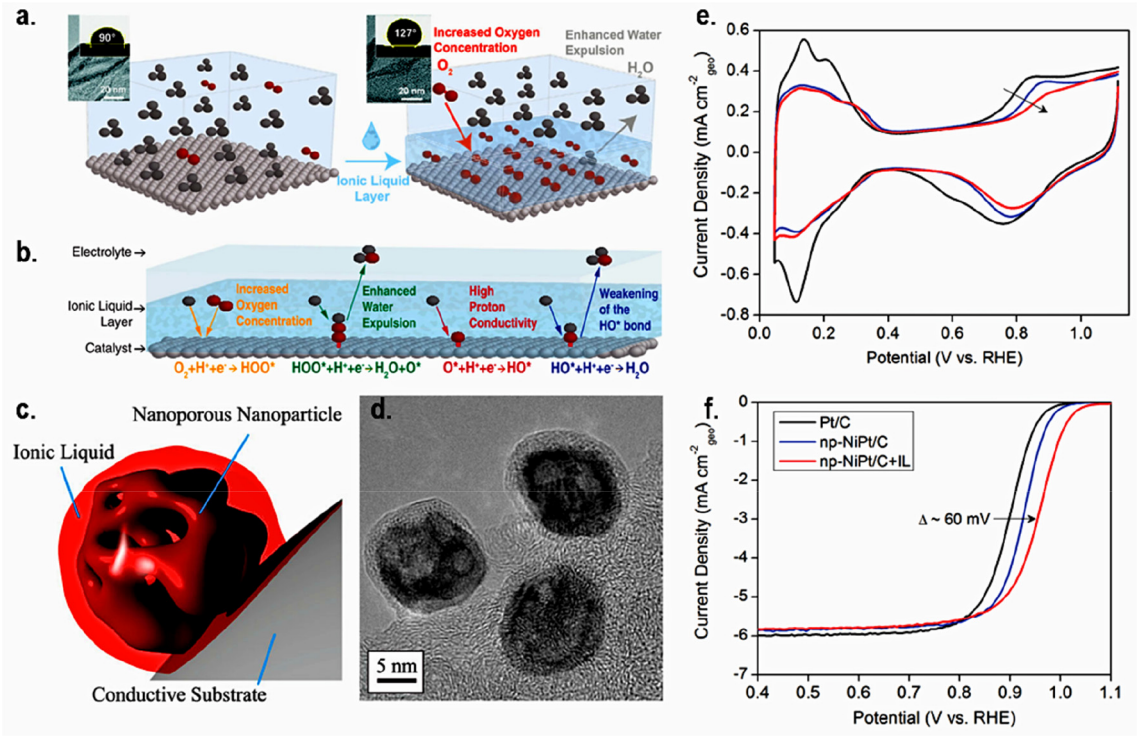

Fig. 6. a. The scheme of an electrocatalyst before and after IL layer addition (inset pictures are the corresponding TEM images of N/C catalyst. Adapted with permission [74]. Copyright 2017, RSC publishing group. b. The scheme of ORR on the catalyst in the presence of the IL layer. Taken from [74], copyrights 2021. WILEY-VCH publishing group. c. Illustration of the nucleus of NiPt NPs encapsulated by ILs. d. HR-TEM of NiPt NPs/C encapsulated with [MTBD][beti] IL. e. CVs, and f. LSVs for the 20% Pt/C, np-NiPt/C, and np-NiPt/C + [MTBD][beti]. Taken from [75], copyrights 2013. WILEY-VCH publishing group.

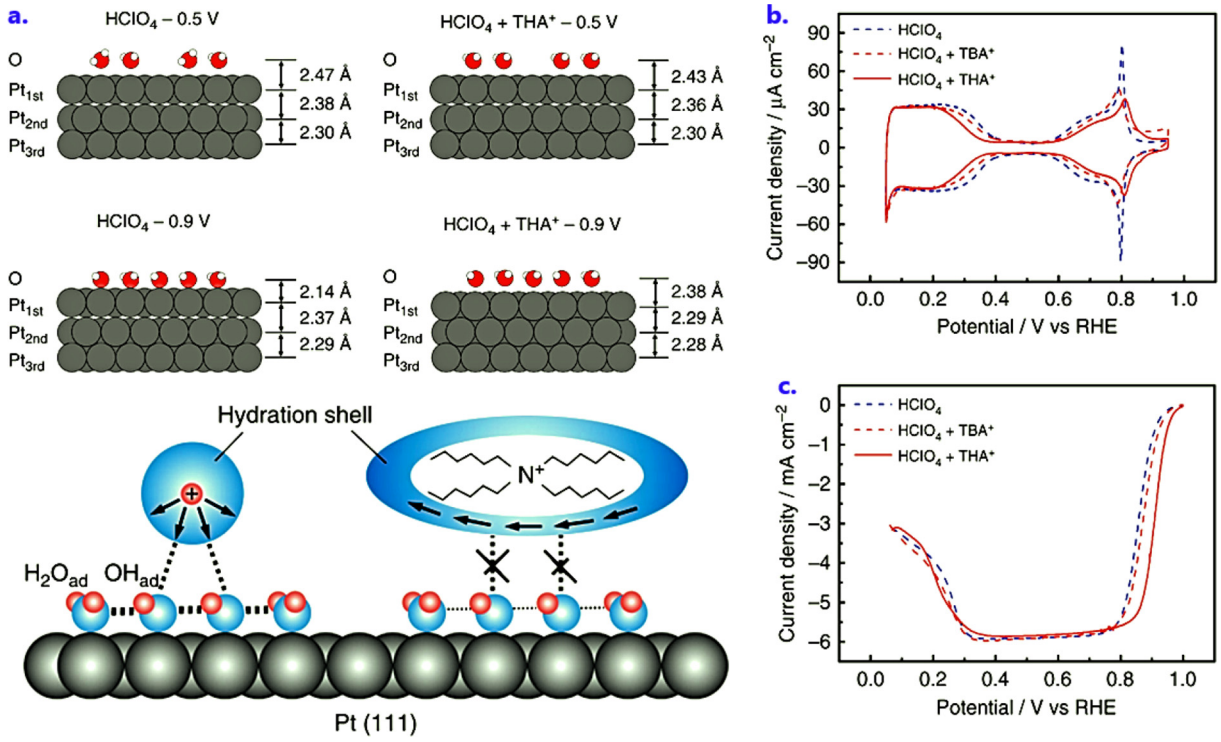

Fig. 7. a. At 0.50 V and 0.90 V versus RHE, schematic models of the interfacial structure of Pt(1 1 1) with and without 10^{-6} M tetra-n-hexylammonium cation (THA^+) saturated with Ar were created. And here is a diagram showing the interfacial hydrated cations and the hydroxide species that have been adsorbed. Two different cations, one hydrophilic and one hydrophobic.

sitating the development of alternative approaches. Another effective strategy for improving ORR electrocatalysis has recently been demonstrated to involve rationally modifying the catalytic metal-ILs interface. Using the ILs, higher oxygen concentrations can be achieved at the catalytically active metal surface as compared to bulk liquid media [73]. It serves as the foundation for these kinds of interfaces. Metal surfaces are better able to conduct ORR due to the existence of a high concentration of surface O_2, particularly in the low overpotential zone. For this reason, high O_2 solubility and high H^+ or OH^- conductivity is required for the ILs to ensure that the ORR intermediates are present at the catalytic surface, as well as a highly hydrophobic catalyst surface to remove water as an ORR by-product from the active site (Fig. 6a-b) [74].

To achieve the superior ORR, *Erlebacher* pioneered research and designed the active metal-ILs composite interface catalyst (PtNi alloy-[MTBD][beti]) (Fig. 6c-d), using the nano-porous alloys and protic ILs[75]. Because of the confinement effect of nano-pores and capillary forces, controlled reactions were made possible during operation. This catalyst displayed superior ORR activity in terms of highly positive half-wave potential and high current density in an acidic electrolyte (Fig. 6e-f). The elimination of H_2O is aided by ILs, which increase the concentration of reactants at the active site, reduce the binding of the HO* intermediate, and increase the H^+ conductivity. There is no doubt in my mind that this composite catalyst can boost the performance of PEMFC. Pt_3Ni nanoframes coated with an ionic liquid showed much higher ORR activity than Pt_3Ni nanoframes that were not coated, as was found in another study [75].

On the other hand, both the solvent and electrolyte ions can affect the catalytic activity of the catalysts. Such solution species, which come from the electric double layer (EDL) at the electrode/-electrolyte interface, and play a crucial role in regulating the ORR activity on Pt surfaces in a considerable way [76]. Adsorption of anions, such as halide and sulfate ions, on the Pt surface, has been shown to drastically impair ORR performance. To produce adsorbed hydroxide (OH_{ad}) on platinum surfaces, it is necessary to expose them to electrolytic solutions that interact with platinum very weakly. The stability of OHad is governed by the surface structure and electrical state of the substrate. In order to activate the ORR, one must first modulate OH_{ad}, which acts as an inhibitor of the ORR [77]. These non-covalent interactions, including hydrogen bonding and electrostatic interactions, maintain certain hydrated cations at the outer Helmholtz plane (OHP) in the EDL [78]. The adsorption equilibrium and its potential are shifted by non-covalent interactions in the EDL. The ORR activity of Pt(1 1 1) increases exponentially as the hydration energy of the OHP cations decreases, and the activity in CsOH is greater than in LiOH (Fig. 7a) [79]. The ORR is deactivated by cations that have a strong affinity for oxygen species, such as Li^+, which has the effect of significantly stabilizing OH_{ad} in the solution. It is vital to adjust the structure and hydrophobicity of the interfacial cations in order to increase ORR activity (Fig. 7b-c) [79].

Within the hydration shell, arrows represent the water dipole's direction of travel. Pt is shown in grey spheres, oxygen in blue spheres, and hydrogen in pink spheres in this illustration. b. The CVs and c. LSVs for at Pt(1 1 1). Reproduced with permission [79]. Copyrights 2018, Nature publishing group.

In acidic solutions, hydrophobicity management is essential in the utilization of proton-exchange membranes in PEFCs. The hydrophobicity and interfacial structure of tetraalkylammonium cations (TAAs) may be manipulated by the chain length of the alkyl groups. Changes in alkyl chain length can have a profound effect on TAA^+'s hydration structure. The ORR activity on single-crystal Pt electrodes in an acidic electrolyte containing TAA+ with varying alkyl chain lengths has been studied in this study. As part of this investigation, in situ measurements of X-ray scattering and infrared (IR) spectroscopy have also been made [79].

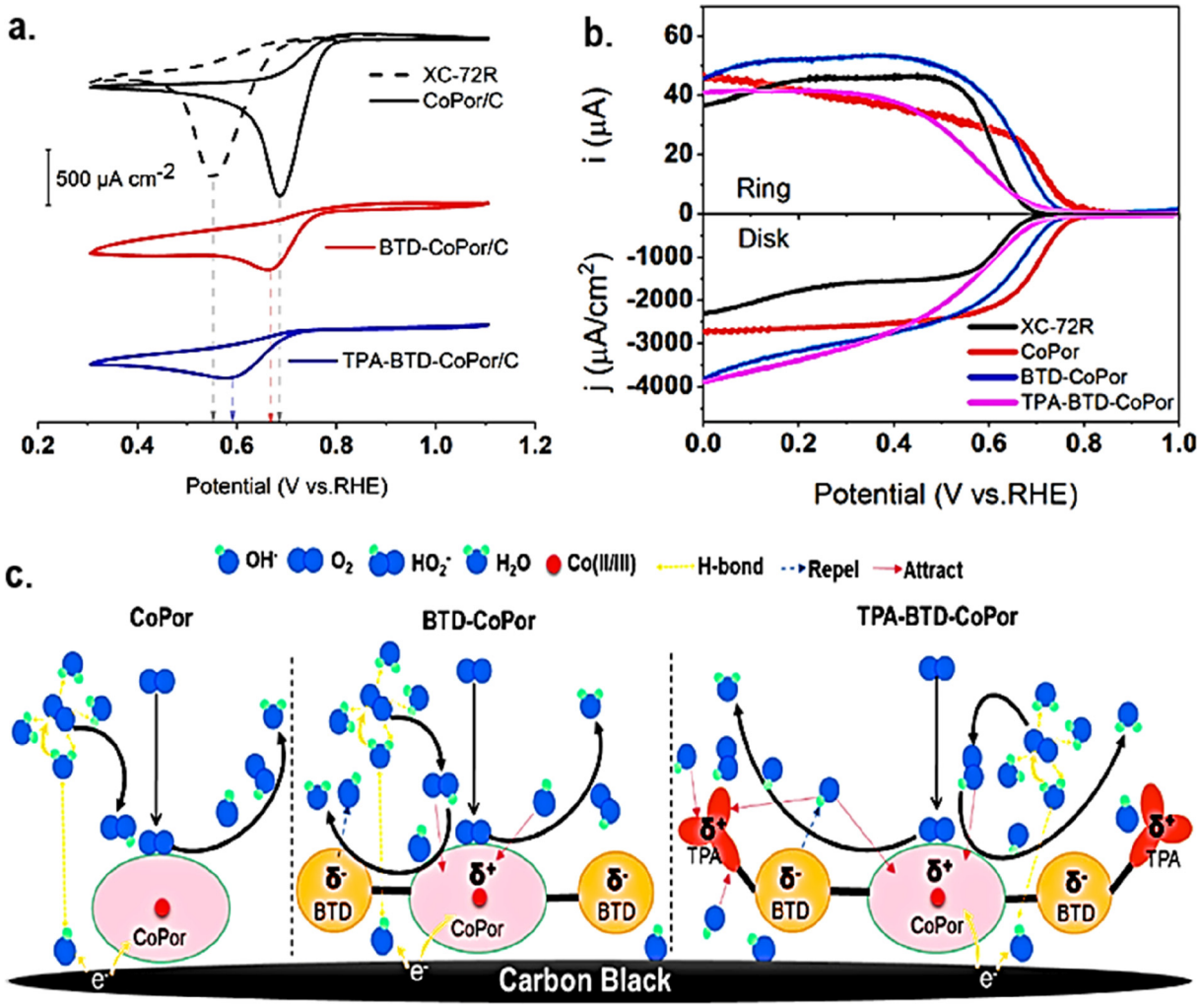

Fig. 8. a. CVs of the investigated catalysts. b. RRDE responses for the catalysts. c. Mechanism of interfacial as well as intermolecular charge transfers for the catalysts, which were designed for the investigations. Taken from [81], copyrights 2021, Elsevier publishing group.

3.5. Controlling the interfacial charge transfer

When designing electrode materials, it is crucial to address the interfaces between the electrode surface and the electrolytic solution, because the bulk of electrolytic reactions actually occurs at the interfaces, which serve as sites for the association of reaction intermediates and electrons. This has been made feasible by the logical design of their microstructures, as well as the chemistry of interfaces, altering the features of triple-phase boundry [80]. The investigations revealed that the ORR kinetics may be improved by producing O-vacancies, which increases the interfacial charge transfer and, as a result, lowers the activation energies for the generation of reaction intermediates. Therefore, the construction of such microstructures, which grow at the interfaces, is crucial for ORR kinetics, and novel manufacturing approaches are required to effectively produce such structures.

Another example of the control of interfacial charge transfer was reported by. Xu et al., considering molecular systems. They suggested that the substituents can affect the ionic state distribution of a porphyrin (Por), which in turn modifies the mechanism of charge transfer at the catalytic interface. They investigated the ORR activity of three different Co-Porphyrins, with the phenyl, 2,1,3-benzothiadiazole (BTD), and BTD-triphenylamine (TPA) substituents at the 5,15-position, (CoPor, BTD-CoPor and TPA-BTD–BTD–CoPor) [81,82]. The results indicated that both the substituted Co-porphyrins displayed improved ORR current density, however, both substituted Co-porphyrins displayed less positive formal potential as compared to CoPor/C (Fig. 8a-b). The e-withdrawing feature of BTD led to an enhanced current density, they argued that the difference in ORR potential was driven by the electronic structure and the generated partial charge effect [83]. Fig. 8c shows a mechanism of interfacial as well as intermolecular charge transfers for the BTD-CoPor/C and TPA-BTD-CoPor/C in alkaline media. These results highlighted the significance of the intramolecular charge transfer to affect the catalytic reaction as well as the limitations of leveraging the TPA structural merits to accelerate the interfacial charge transfer in an alkaline environment. In another work, Lee et al. found a considerable improvement in ORR kinetics due to the creation of defects at the interface [80]. In this work, contiguous coatings of the thin film-like layer with thicknesses of up to 8 nm were applied to the porous YSZ scaffold. The ratio of Y_2O_3 mole from 0 to 20 mol% appropriately regulated O-vacancies. These O-vacancies at interfaces were critical in accelerating ORR dynamics [84,85], as well as promoting charge transfer and ionic incorporation at the interface[86]. These findings show that the tailoring of interface defects by a facile wet chemistry-based strategy may considerably boost the ORR kinetics of the materials.

3.6. Creating the conductive interface

Nanocarbons, such as graphene (Gr), carbon nanotubes (CNTs), carbon black (CB), and graphite-carbon nitride (g-C_3N_4), are of significant interest in material research because of their unique properties, such as large surface area, conductivity, and chemical and mechanical stability. In particular, these are more advantageous in electrocatalysts [87,88] due to their conductive and defective structure, N-rich carbon backbone, and their ability to accommodate a variety of metals. On the g-C_3N_4 plane, its obvious structural defects, may facilitate O_2 absorption and display good activity. However, g-C_3N_4's insignificant electrical conductivity inhibits its catalytic activity [89,90]. This problem may be rectified by injecting a large number of free electrons into g-C3N4 via metallic dopant components, enhancing the charge ability as well as the catalytic performance of g-C_3N_4. Moreover, N-doped aromatic moieties are reported to affect the electronic state of metal NPs on the surface of nanocarbons, as a basic foundation for building conductive channels and modifications of the ORR energy barriers for further enhancement of electrocatalytic performance. A number of methods have been utilized to create conductive channels, but gamma radiation is considered to be the most promising approach due to its high efficiency, non-toxicity, and eco-friendliness. In addition, this method allows chemical reactions to take place at any temperature and pressure, in absence of catalysts, promoters, or cross-linking agents. The penetration of redox species is also possible using this approach, enabling the initiation of ORR [91,92,93]. For instance, the development of a novel strategy for the construction of conductive channels between the PtNPs and g-C_3N_4 support was reported by Xiang et al., [93] (Fig. 9a). Then, the as-prepared nanocomposites CN/Pt were used as an electrocatalyst for ORR. During ORR, the CN/Pt catalyst demonstrated a modest Tafel slope with a rapid 4e-transfer route. The ORR activity over the CN/Pt electrode is much better than that of conventional Pt/C electrode and the majority of published g-C_3N_4-based electrodes (Fig. 9b-c). Fig. 9d-e showed the systematic interfacial e− transfer mechanism in the pristine g-C_3N_4 and CN/Pt nanocomposite during ORR. Fig. 9f shows the chemical model for g-C_3N_4, which has conductive interfaces. Experiments have shown that the metal-support contact can be used to quickly transfer charge between PtNPs and g-C_3N_4. This shows that this method can be used to improve the catalytic performance of g-C_3N_4 [93,94].

3.7. Changing the solvent composition

The solvent has a stabilizing effect on a specific intermediate in the ORR process. The dielectric constant of a solvent has been found to alter the binding strength of ORR intermediates on Pt (1 1 1), and adopting the solvent with the optimal dielectric constant may boost ORR activity [95]. Federico et al. [96] investigated the adsorption strength of ORR intermediates on a variety of metal centers, including Cr, Mn, Fe, Co, Ni, and Cu, utilizing metalloporphyrins in a variety of solvents. Results showed that the covalence of metal active centers systematically broke the linear relationship between ORR intermediates under vacuum by strengthening M-OOH bonding with simultaneous modification of adsorbate solvation in solution. This phenomenon was dependent on the covalency of the metal–adsorbate bondings in solution under vacuum and solvated conditions (Fig. 10(a-b)), the E_b^{*O}, E_b^{*OH}, and E_b^{*OOH} were shown to have similar scaling relationships. The covalence effects of metal centers on *OH and *OOH adsorption is illustrated in Fig. 10c (plot of differences in E_b^{*O}, E_b^{*OH}, and E_b^{*OOH} under vacuum vs. electronic charges), and Fig. 10d (solvation energies vs. electronic charges). The deviations from ideality rise in opposing direc-

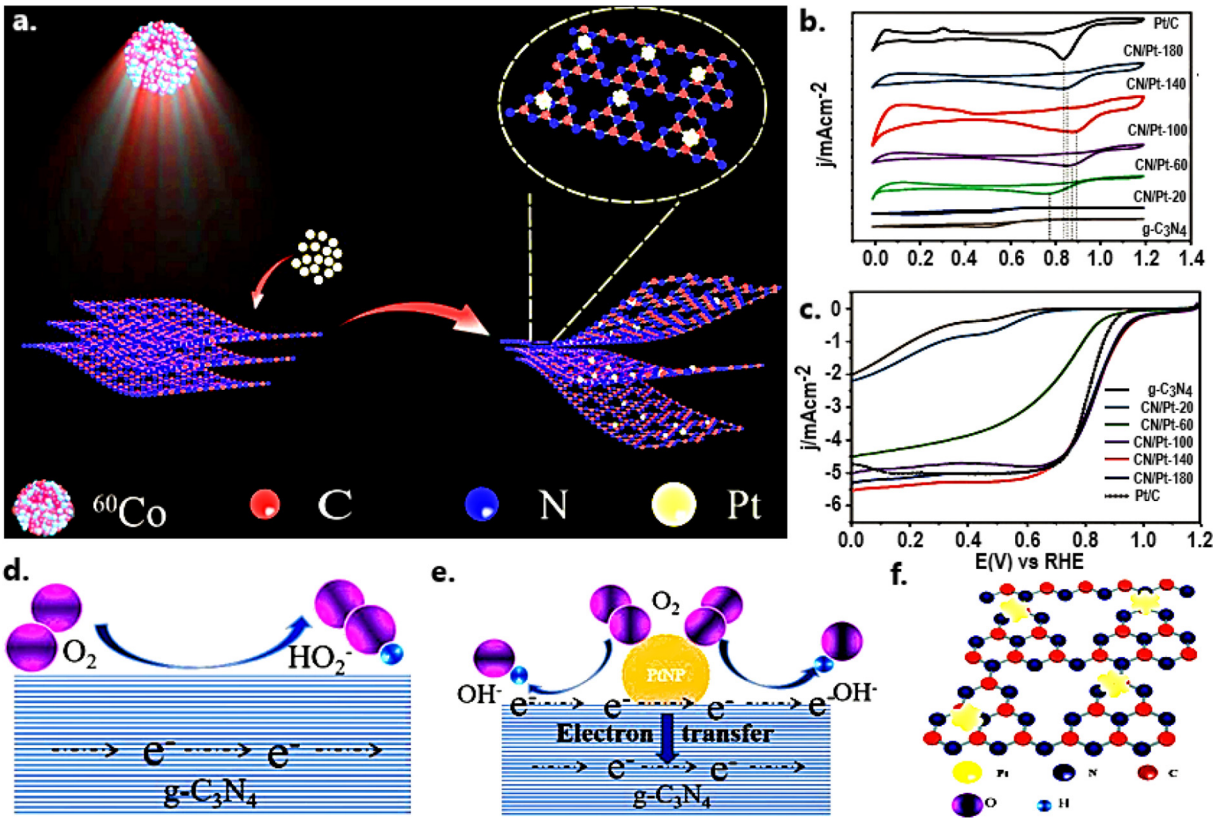

Fig. 9. a. A schematic representation of CN/Pt synthesis, b. CV and c. LSVs of the various CN/Pt samples and Pt/C catalyst. d. Interfacial e− transfer mechanism in pristine g-C_3N_4, and e. ORR mechanism for the CN/Pt materials, f. chemical model for g-C_3N_4, having conductive interfaces. Taken from [93], copyrights 2020, ACS publishing group.

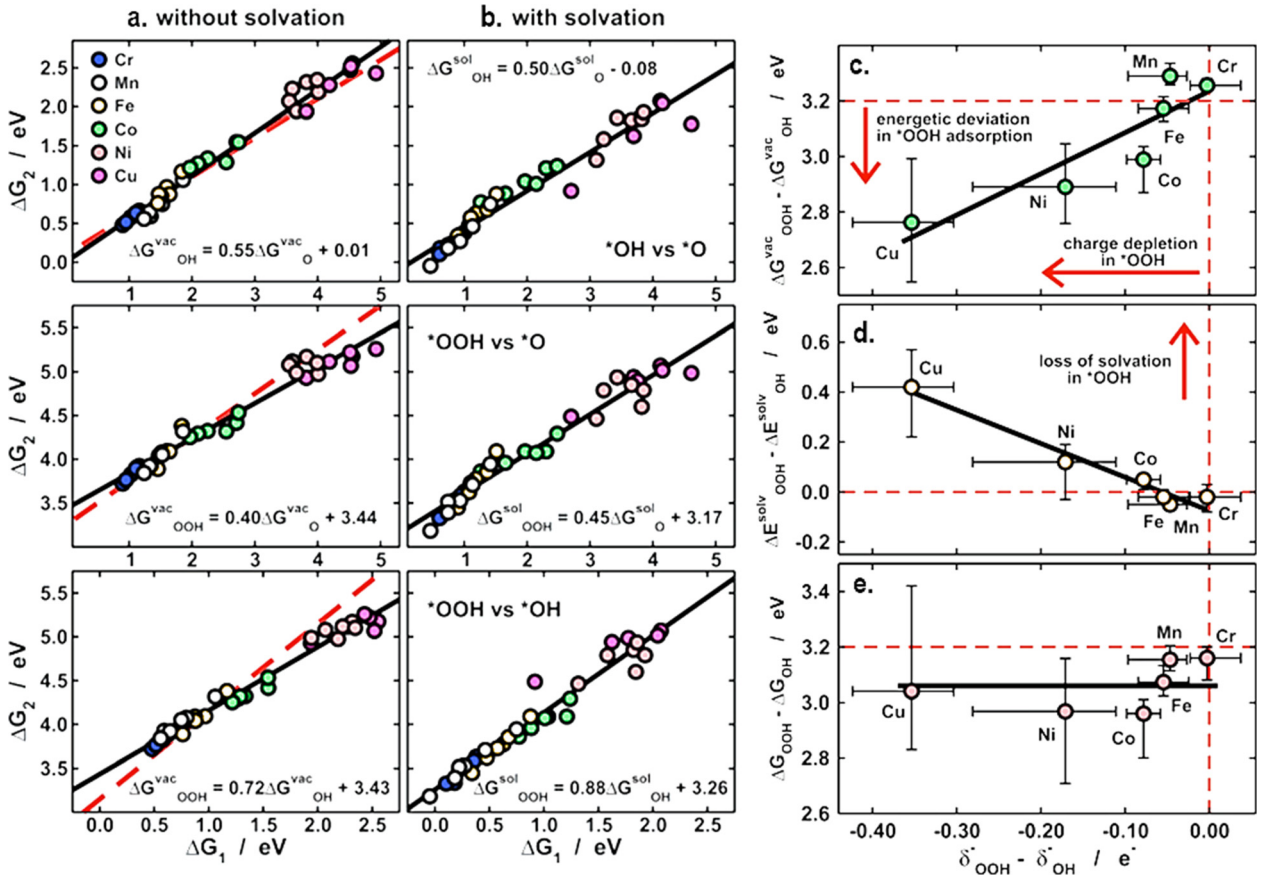

Fig. 10. Scaling relations between the E_b^{*O}, E_b^{*OH}, and E_b^{*OOH} under a. Vacuum, and b. Solvated. Covalence effects of metal sites on ORR intermediates adsorption, c. plot of differences in E_b^{*O}, E_b^{*OH}, and E_b^{*OOH} under vacuum vs. electronic charges. d. solvation energies vs. electronic charges. e. The differences in solvated adsorption energies are nearly constant (3.1 eV). When * OOH and * OH have equal charges and solvation energies and a 3.2 eV energy separation, the dotted lines in (c – e) represent the ideal situation. Taken from [96]. Copyright 2017, RSC publishing group.

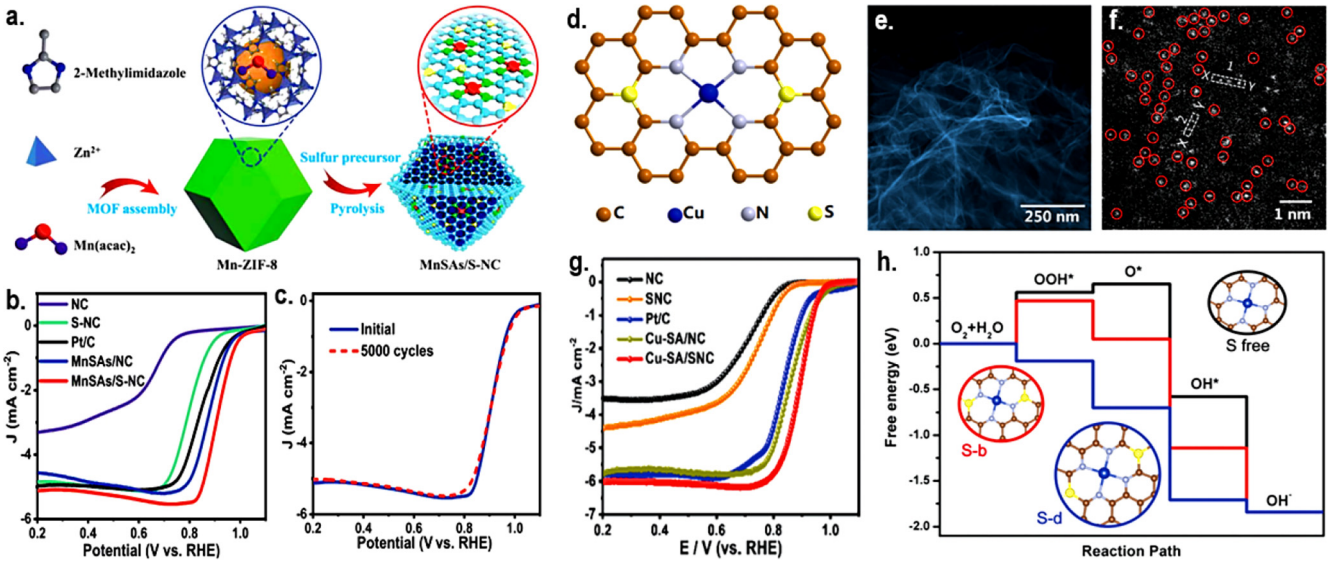

Fig. 11. a. Schematic graphic for MnSAs/S–NC synthesis. b. LSVs for the MnSAs/S–NC, MnSAs/NC, S–NC, NC and commercial Pt/C catalysts. c. LSVs before and after 5000 CV cycles for MnSAs/S–NC. Taken from [100]. Copyright 2020, RSC publishing group. d. Representation of Cu-SA/SNC active sites, e-f. TEM images Cu-SA/SNC active sites, g. LSV curves of catalytic samples, and h. ORR mechanism on Cu-SA/SNC active sites. Taken from [101]. Copyright 2019, RSC publishing group.

tions while moving from Cr to Cu, the difference between their respective solution adsorption energies is practically constant (3.1 eV) (Fig. 10e). As shown in Fig. 10(c-e), there is an ideal condition where * OOH and * OH have equal charge and solvation energies, as well as a 3.2-eV energy gap between them. Solvation is, therefore, a deciding component that must be considered while

aiming at breaking scaling relations in the solutions. These findings suggest that to a certain extent, scaling relations dictate the catalytic activity, but other factors, such as solvent selection, have the potential influence on it [96,97].

3.8. Modulation of atomic interfacial effects in single or dual atom catalysts

In addition to the previously stated interfacial approaches for the design of catalysts, atomic interface engineering has also been considered as a viable strategy to regulate the ORR activity of single or dual atom catalysts (SACs or DACs) [98 99]. For instance, Huishan Shang et al., [100] reported an interface approach to developing a MOF-derived S-doped Mn–N–C SAC (Fig. 11a). The operando X-ray absorption spectroscopic investigations revealed that isolated Mn-N bond-length extended the low-valence state of Mn in S-doped Mn–N_4 SAC moieties, which acted as ORR active sites. This catalyst displayed excellent ORR activity, having 0.916 V vs. RHE half-wave potential (Fig. 11b) as well as significant durability (Fig. 11c) in an alkaline environment. This work opens the door for the development of ORR catalysts that may be tailored to the local environment of catalytic active sites [102,103].

In a similar way, Zhuoli Jiang [101] reported atomic interfacial engineering to improve the ORR performance of Cu-based SACs, by incorporating S-atom in the local environment of the Cu site (Cu-SA/SNC) (Fig. 11d). The TEM pictures of Cu-SA/SNS clearly indicated the Cu-active sites in the S-doped carbon matrix (Fig. 11e-f). Further, studies using DFT calculations combined with XAFS techniques revealed that isolated bond-shrinking in Cu(+1)–N_4–C_8S_2 atomic interface moiety, with a low-valence state of Cu, acted as ORR active sites. An important role in improving ORR activity (Fig. 11g) is played by a synergistic effect between Cu-components and carbon support at the atomic interface, which is adjusted by altering the free energy of ORR intermediates. Fig. 11h showed the proposed ORR mechanism on Cu-SA/SNC catalyst. As an alternate way of designing enhanced oxygen electrode materials, this approach may present a unique approach to boosting the catalytic performance of SACs. This new atomic interface impact for SACs may serve to boost their ORR performance [104,105,32].

Synergistic catalysts, on the other hand, are increasingly being developed with more complicated active sites, such as diatomic or multi-atomic sites, and atomic interfaces, in which distinct atomic centers might potentially catalyze complex processes that are beyond the capabilities of SACs. The combined effect of several centers might improve the catalytic activity even further. Constructing these elaborate sites may also alter the reaction products' selectivity for different types of reactions. For example, on single Pt atoms, the ORR reaction prefers the 2e pathway, which results in the formation of H_2O_2. However, on Pt NPs or alloys, the ORR reaction favors the 4e pathway, which results in the formation of H_2O, due to the synergistic interaction between neighboring metal atoms. To achieve high-performance ORR catalysts, it is, therefore, possible to create nearby active centers as catalytic sites at the atomic level, which is a practical technique. A lot of obstacles exist in the construction of these complex catalytic sites at the current time; scientists must investigate approaches for controlling the chemical identities, loadings, bonding, and coordination configurations with more accuracy [106 107 108 109].

3.9. By introducing functional groups/H^+-relay groups at the interface

In nature, certain noncovalent interactions between enzymes and reaction intermediates, known as the secondary coordination sphere effect, are found to be capable of controlling the overall enzyme activity as well as selectivity. On the basis of this approach adopted by nature, various papers indicated that the O-O connection has been broken by the addition of H^+-donor/acceptor groups that stabilize *OOH rather than *OH because of regulated H^+-activity by these groups. Additionally, porphyrins and their derivatives seem to be appealing due to their structural similarity to metalloenzymes. As an example, the synthesis of a graphene-porphyrin (Por) metal–organic framework (MOF) architecture (Fig. 12a) was accomplished by employing pyridine-

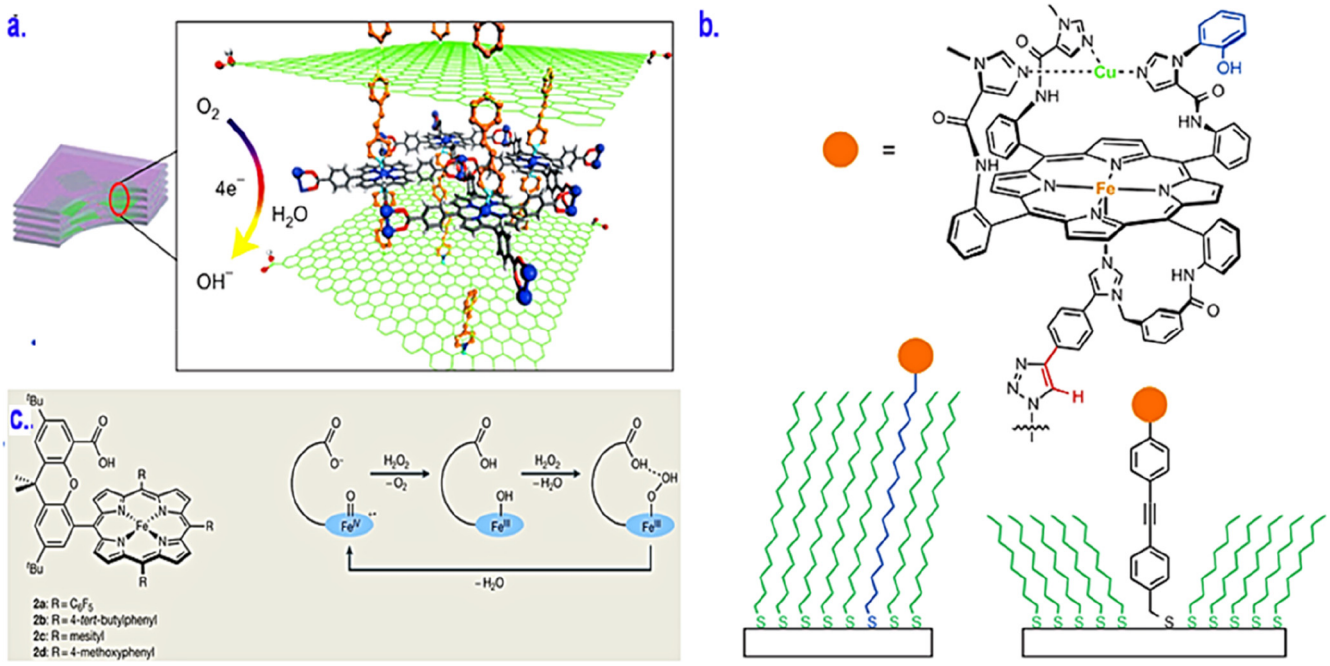

Fig. 12. a. The graphical representation of graphene–porphyrin-MOF-composite for ORR. Taken from [110], Copyrights 2017, ACS publishing group. b. The typical model of cytochrome *c* oxidase for ORR. Reprinted with permission [112], copyright 2007, American Association for the Advancement of Science (AAAS) publishing group. c. Porphyrin having proton donor groups, hangman model of porphyrin with proton relay groups. Taken from [113], Copyrights 2013, ACS publishing group.

functionalized reduced graphene oxide (Py-rGO) and iron-porphyrin (Fe-Por)[110]. Specifically, the presence of Py-rGO significantly enhanced the electrocatalytic activity of the Fe-Por and interacted with it in a synergistic manner. This resulted in a facile 4e− ORR, and thus opens the door to a potential alternative to Pt-based materials for FCs. Several recent studies have also outlined the promising future of tetrapyrrole-functionalized 2D-nanocarbons [111].

Moreover, several multifunctional structures were also investigated, which combined the features of solution-dispersed GO and Por to enhance their catalytic activity. It has been discovered that the formation of a covalent amide bond between TPP-NH_2 species [112] and GO in DMF leads to the formation of a novel material that is processable in organic solution (Fig. 12b). The idea behind this work can be used to design ORR electrocatalysts, which will offer strong interfacial interactions to control the H^+-activity, thereby, improving the ORR activity. In other work, the dangling of carboxylic groups, which acted as proton donor/acceptor groups, was created in the meta-position of porphyrin. This enhancement in ORR activity was attributed to the control of H^+-activity at the molecular interface (Fig. 12c). Therefore, it is possible to circumvent the scaling relation and boost the catalytic efficacy of modified molecular catalysts by using near proton donor/acceptor groups [113].

A simple interfacial strategy to prepare a nanocomposite, CoPc supported on CNTs as an ORR catalyst with a hydrophobic ionic liquid layer coating, was reported by Zixun et al. [114] (Fig. 13a). High-resolution TEM images clearly indicated the hydrophobic IL layer coating around the CNTs (Fig. 13(b-c)). They also proposed a relationship between the thickness of the ionic liquid layer on the catalyst surface and the ORR activity of the catalyst. In contrast to the aqueous system, it was discovered that O_2 solubility was greater in the IL system, resulting in an enhanced surface layer of O_2 near the active catalyst sites, which improved the thermodynamics of the ORR system. The results indicated that the ORR intermediate H_2O_2 could be effectively rejected by the ionic liquid layer, and as a result, it impeded the breakdown of water into H_2O_2 by virtue of its strong selectivity towards 2e− ORR (Fig. 13(d-e). It is also possible to boost H_2O_2 selectivity by using hydrophobic IL, which efficiently deflects the H_2O_2 molecules away from the catalytic surface. In addition to improving ORR performance, such interfacial effects open up new avenues for electrocatalytical processes by allowing them to take place in different microenvironments at the active site.

Yao Ma et al., [115] suggested that the activity and stability of heterostructures with significant coupling effects between different components can be greatly improved, developing a heterostructured bimetallic phthalocyanine catalyst (FePc/CoPc HS) with a heterogeneous distribution of metallic components (Fig. 13f). This heterostructured catalyst, FePc/CoPc HS, displayed excellent ORR performance as compared to parent FePc and CoPc molecules (Fig. 13g). The results of fine structure analysis combined with computational studies on the FePc/CoPc HS heterostructure revealed the elongation of Fe-N bond length in FePc and increased electron density around Fe active sites, thereby decreasing the energy gap between HOMO and LUMO, which was responsible for the ORR improvement. In another work, Yan Li et al., [116] investigated the ORR of CoPc and its derivatives at the interface of polarised water/DCE. They hypothesized that H^+/e^- transfer processes actually occurred at the interface between two phases, where the Galvani potential difference and the catalyst's molecular properties governed H^+ transfer and e^- transfer events, respectively (Fig. 13h). There is no influence of the substrate on the electrical properties of this biphasic catalyst. This was the first time that electrocatalytic ORR by phthalocyanines at the liquid/liquid interface had been studied. These works pro-

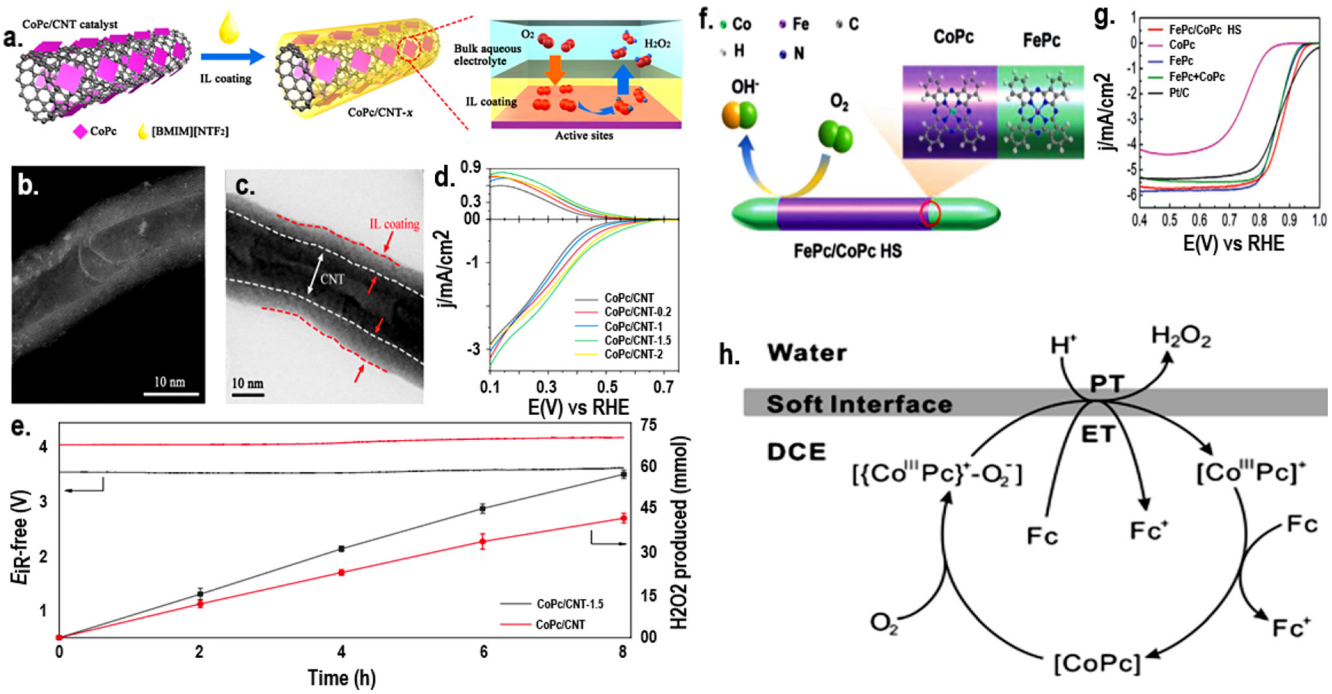

Fig. 13. a. schematic illustration of IL coated CoPc/CNT synthesis and its H_2O_2 selectivity. b-c. High-resolution TEM images of IL coated CoPc/CNT catalyst. d. LSV curves of the CoPc/CNT and CoPc/CNT-x catalyst samples. e. Chronopotentiometric curve for the H_2O_2 production at IL coated CoPc/CNT catalyst. Taken from [114]. Copyrights 2022, Elsevier publishing group. f. Schematic graphical representation of FePc/CoPc HS. g. LSV curves of FePc-based catalyst samples. Taken from [115]. Copyrights 2020, Wiley-VCH GmbH, Weinheim publishing group. h. Systematic illustration for the H^+ pump mechanism controlled by Galvani potential difference for ORR catalyzed by CoPc. Taken from [116]. Copyrights 2020, Wiley-VCH GmbH, Weinheim publishing group.

vide insights into how to change the electronic structure of heterostructured bimetallic phthalocyanine-based ORR electrocatalysts at the interfacial level. [107,117].

3.10. Using conductive support for Bio-inspired molecular catalysts

A family of molecular catalysts, such as metallo-phthalocyanines (MPcs), metallo-porphyrins (MPs), and their derivatives are ORR active, but, owing to de-metalation, these catalysts lose their activity. In this regard, the covalent or non-covalent attachment of these molecular catalysts to conductive materials support, such as nano-carbons and metal oxides, not only increases their activity due to interfacial electronic communication between catalyst and support but also improves their stability in the electrolyte. Therefore, the synthesis of molecular catalysts on support composites is an appealing interfacial technique for the development of low-cost and effective electrocatalysts [118–122]. For instance, Hijazi et al. [123], conducted a Hay-coupling reaction between CoP molecules, resulting in a covalent network due to polymerization of cobalt porphyrin (CoP) molecules, which got adsorbed on MWCNTs surface. The polymeric composite, MWNT-CoP displayed superior ORR performance as compared to monomeric CoP in 0.5 M H_2SO_4 electrolyte, following 4e− transfer ORR. Due to the cooperative effect of multiple π-π stacking between CoP moieties and MWNT's surface and the covalent bridge between CoP molecules on MWNT's surface, the MWNT-CoP composite attained high stability. In a similar work, FePc was gathered on a pyridine (Py)-functionalized SWCNT to produce axial pyridine-coordinated FePc (FePc-Py-CNTs) [124]. This catalyst showed excellent ORR activity as compared to the Pt/C catalyst, displaying 35 mV vs. RHE anodic shift in half-wave potential in basic media, following 4e− transfer ORR. This enhancement in ORR activity of FePc can be attributed to the interfacial effect of CNTs via axial Py-coordination with FePc. Similarly, CoPc-Py-CNT composite has been reported through anchoring of CoPc on CNTs surface, and was found to show 4e− ORR, while CoPc exhibited 2e− ORR [125]. Theoretical results indicated that Py connected at CNTs interface acted as fifth coordination with CoPc and stabilized Co in the low spin state with one unpaired electron, which increased the O2 binding energy with Co, endowing the initiation of O-O bond rupture directly.

By Jianshe Huang et al. [126], an explicit five-coordinated Fe–N connection was demonstrated in a 3D graphene aerogel (GA) supported FeN5 composite. Pyridine groups (FePc/AP-GA) were used to covalently graft FePc molecules (FePc/AP-GA) onto graphene (Fig. 14(a-b)). Its half-wave potential in an alkaline electrolyte was 0.035 V (vs. Hg/HgO), which is significantly greater than that of the benchmark Pt/C catalyst and other pyrolyzed or nonporous metal catalysts (Fig. 14c). Its ability to retain a high current density at +0.1 V, as well as its extended lifespan and excellent resistance to the effects of methanol poisoning, was an additional attribute of this composite material. The characterization and theoretical studies reveal that the modified coordination and electronic environment of the Fe-active site in FePc/AP-GA composite due to fifth coordination facilitate the adsorption of ORR intermediates, resulting in ORR activity as well as durability enhancements.

For the first time, attaching axial ligand with FePc, Jia Guo, et al. [127], prepared a nanostructure via a graphene-assisted colloid chemical reaction. (Fig. 14d) As compared to traditional Pt/C catalyst, this nano-architecture exhibited more positive onset potential (1.0 V vs 0.97 V) as well as half-wave potential ($\triangle E_{1/2}$ = 100 mV) towards ORR in an alkaline environment. In addition, this catalyst also displayed better durability as compared to Pt/C (Fig. 14e). The analytical data indicated that FePc was axially coordinated through a Fe-O-C connection with graphene support, and therefore, the redox couple Fe(III)Pc/Fe(II)Pc acted as ORR mediator. Further, the theoretical investigations showed that four- and five-coordinated Fe atoms displayed synergistic ORR as supported by experimental studies (Fig. 14f). The work opened an interesting perspective on the synthesis and utilization of metallo-porphyrins and metallo-phthalocyanines and their derivative for the development of SACs-based electrocatalysts for ORR.

Further, Zhou et al., [128] grafted the FeP derivative, (5,10,15,20-tetra(pentafluorophenyl) iron porphyrin) (FeF20TPP), onto the MWCNTs in which the Fe porphyrin derivative was coordinated with covalently electro-grafted axial ligands, including

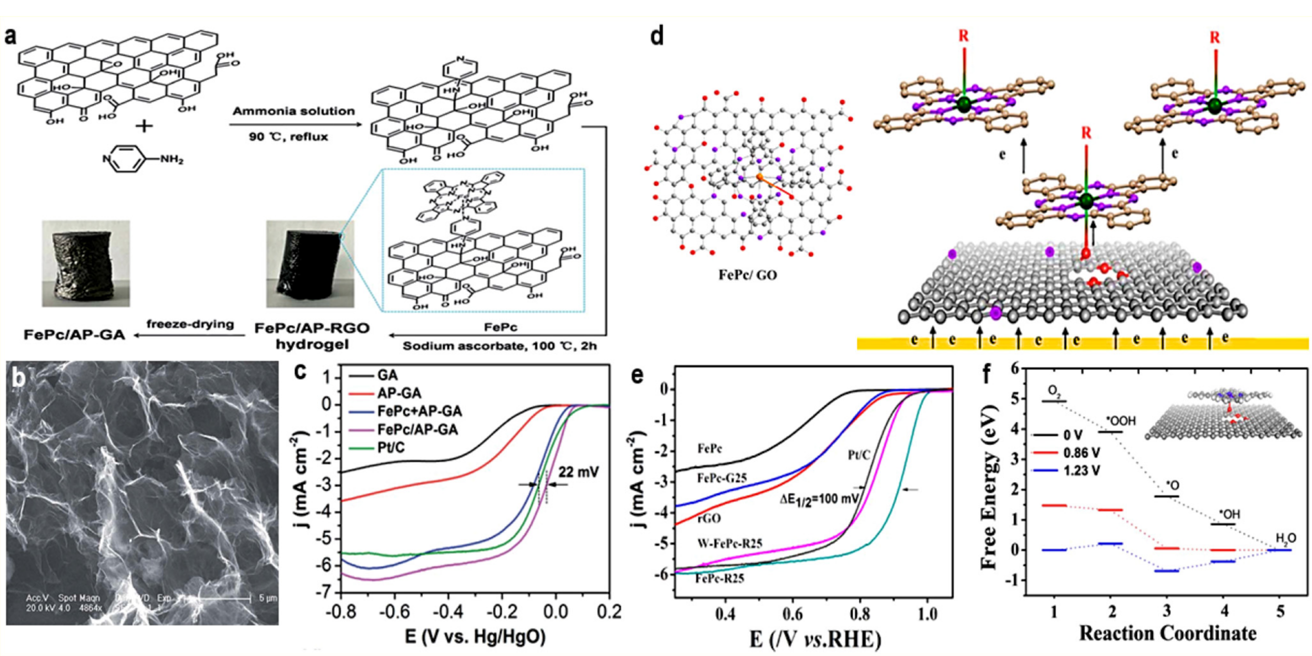

Fig. 14. a. Fabrication process of the 3D FePc/AP-GA composites. b. SEM, and c. LSV curves of prepared samples recorded at 10 mV/s and 600 rpm in O_2-soaked 0.1 M KOH. Adapted with permission [126]. Copyright 2018, RSC Publishing Group. d. ORR mechanism assisted by Fe(II)Pc/Fe(III)Pc redox couple @RGO, e. LSV curves for prepared FePc-based catalysts, f. Gibbs free energy diagram for ORR on prepared catalysts. Adapted with permission. Copyright 2018, Elsevier Publishing Group [127].

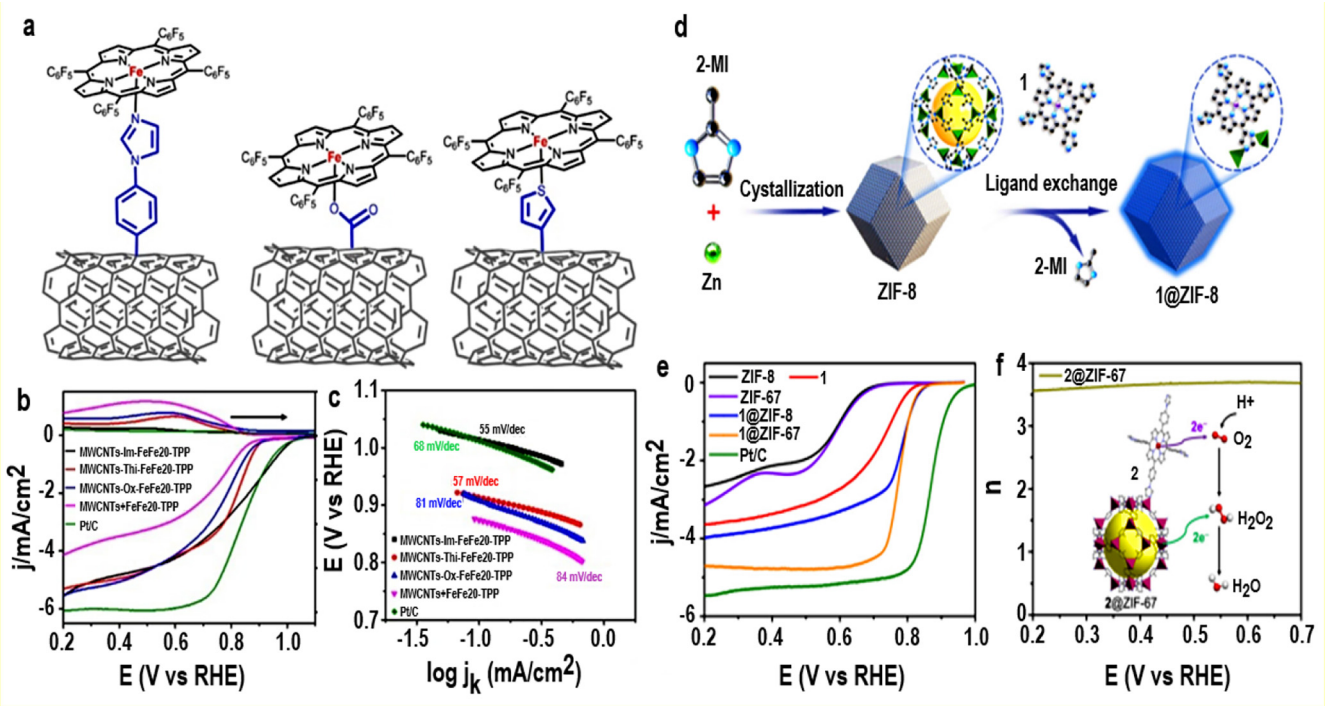

Fig. 15. a. Structural model for MWCNTs-Im-FeF20TPP, MWCNTs-Thi-FeF20TPP, MWCNTs-Ox-FeF20TPP, and MWCNTs + FeF20 TPP. b. LSV curves, and c. Tafel slopes for the prepared samples, and Pt/C recorded at 1600 rpm in O_2-soaked 0.1 M KOH. Adapted with permission [128]. Copyright 2021, Wiley-VCH Publishing Group. d. Grafting 1 onto ZIF-8, 1@ZIF- 8, e. LSV curves, f. ORR mechanism and electron transfer number for 2@ZIF-67, calculated at 1600 rpm, O_2-soaked 0.1 M KOH. Adapted with permission. Copyright 2021, Wiley-VCH Publishing Group [129].

thiophene, imidazole, and carboxylic, on the surface of the MWCNTs (Fig. 15a). Among all, the imidazole-coordinated Fe porphyrin derivative/MWCNTs displayed the highest ORR activity. The highest ORR activity of an imidazole-coordinated Fe porphyrin derivative/MWCNTs catalyst might be attributed to the high electron density transfer to the Fe-site via the N-donor atom of the imidazole ring (Fig. 15(b-c)). This is because the N-donor atom of the imidazole ring is a less electronegative donor than the other O and S-donor atoms. An electro-grafted molecular catalyst preparation approach with activity descriptors that may be applied to the creation of various electro-grafted catalysts for energy conversion is presented in this work. In another work, the Co porphyrin@MOF composite was developed by Liang et al. [129] using MOF as a conductive support for Co porphyrin (Fig. 15d). Compared to Co porphyrin, the ORR activity of this composite was much higher (>70 mV anodic shift in half-wave potential) and selective (4e− ORR). Following 2e− ORR, Co porphyrin reduced O_2 into H_2O_2, which was further reduced at MOF, resulting in a total 4e− ORR ORR (Fig. 15(e-f)). Therefore, controlling the morphology, composition and architecture of new materials, constructing nanocomposites and/or nanohybrids, as well as engineering the surface structures are considered vital to boosting the electrochemical performance of electrode materials for next-generation energy conversion and storage technologies [130–141].

4. Conclusions

4.1. Remarks and challenges

This review covers the progress in interfacial effects-based strategies that have been achieved in tailoring metal surfaces and interfaces to promote electrocatalytic ORR. The interfacial effects can (i) adjust the electronic properties of catalysts via electron transfer, (ii) stabilize the catalysts via interfacial bonding, (iii) accelerate the e− transfer via creating a conductive interface, and (iv) enable the bi-functional adsorption of reaction intermediates. Over the last several decades, a substantial amount of research has been performed to improve mechanistic knowledge of the electrocatalytic behavior of metal surfaces and interfaces, to guide the design of high-performance catalytic structures. Meanwhile, the need to achieve optimal catalytic surfaces on nanomaterials has driven extensive research to create novel nanotechnologies that allow the crystallographic orientation and interfaces of nanocatalysts to be governed logically. As a consequence of these efforts, the ORR electrocatalytic activity, which is inextricably linked to the green and renewable energy achievements, of metallic catalysts, has experienced major gains in recent years. Consequently, the ORR intermediates like *OOH and *OH show a strong scaling link. Therefore, optimizing them on one kind of catalytic site alone is quite difficult. In this regard, a paradigm changes in catalyst design to control the proton activity using interfacial hydrogen bonding could successfully prevent the inherent overpotential that was generated by the adsorption-energy relationships of ORR intermediates. Therefore, the adsorption-energy scaling equations can be circumvented by finding a way around or around them using interfacial engineering. Moreover, combining the computational investigations with materials science as well as interfacial electrochemistry may be the strategy of choice to monitor proton's activity during the electrocatalytic reactions not only for ORR but also for other H^+/e− involving reactions. Based on this fact, the work function of electrocatalysts may be modulated by constructing the interfacial interactions of various components. These interactions can be exploited to reduce the energy barriers to the chemisorption of ORR intermediates, thereby, enhancing the elec-

trocatalytic reaction kinetics. Therefore, the creation of interfacial structure and the knowledge of the mechanism of catalytic reaction are essential for effective design and use in electrocatalytic reactions. On the other hand, the noble metal-supporting materials were used to understand the interfacial effects between the noble metals. The interaction between these metal surfaces and supports was found to be capable of controlling the ORR activity, affecting the binding energy of ORR intermediates. In contrast, if interfacial effects don't play a role in the choice of catalyst and support, the inert support could make the electrocatalytic properties of the catalyst worse.

Besides, it is far more difficult to design electrochemical interfaces than it is to design solid–gas ones. The electrochemical reactions involving multiple e-transfers and intermediates take place on the surface or interface of a catalyst. Therefore, the analysis of solvent layers, ions, and control of H^+-activity and potential is extremely difficult at the molecular level. In this context, the interfacial bond-based approach can be considered the most favorable strategy among all, including strain, and solvent-composition-based strategies to control the catalyst's ORR activity. During electrocatalysis, interfacial bonds get frequently exposed to regulate the re-arrangement of electrons in hetero-interfaces and to trigger the e-transfer from active sites to substrates. As a result, interfacial bonds-based strategies may be utilized to alter the electrical characteristics of interface components, thus enhancing the ability and chemical stability of active sites during ORR intermediate chemisorption.

4.2. Future prospects

Although the interface interactions with electrocatalyst structures play a crucial role in electrocatalysis and a significant amount of research has been performed, there are still certain problems and interesting parameters that require more investigation. The construction of the interface in the majority of electrocatalysts is generally restricted to a chemical combination of two or three constituents. Therefore, future research might concentrate on the development of novel preparation strategies that are simple to implement and scale-up for practical use. Depending on the structure-sensitive of the material, mere exposure to air and/or a realistic reaction environment may be enough to promote surface changes, resulting in the creation of a stable interface structure. The use of materials' sensitive properties to create interface structures cleverly can be regarded as an efficient approach to creating stable and high-efficiency electrocatalysts. Moreover, the understanding of the genuine active sites in electrocatalysis is also critically important.

Researchers may be able to rationally design catalysts in the future if they can determine the true causes of interfacial effects in the future. It is often believed that improved electrocatalytic performance of supported catalysts is due to the strain effect, the establishment of an interfacial bond, and the production of conductive interfaces as the primary factors. Indeed, since multiple interfacial effects often manifest themselves at the same time, it is difficult to distinguish between the contributions of distinct interfacial effects. Apart from that, the nature of the electrocatalysis processes adds to the difficulty of this problem. When the same reaction is carried out under various environmental circumstances, the interfacial effects on electrocatalytic activity may be varied owing to the diverse reaction processes, resulting in varying electrocatalytic activity for the same reaction. In addition, the mechanism of some electrocatalytic processes continues to be a matter of controversy. Therefore, to study the interfacial effects, new methods for constructing catalysts on a monolayer of a substrate with well-defined interfacial site distributions as well as advanced characterization techniques will be required. There has been a lack of studies for the development of electrocatalytic processes owing to the limitations of synchrotron-based technologies, which are crucial for the identification of actual catalytic active sites on the surface of electrocatalysts. Moreover, the advanced version of X-ray-based techniques is anticipated to be very useful for the effective and ultrafast detection of catalysts and reactions due to their high sensitivity. As far as highly efficient electrocatalytic processes are concerned, the coherent and tunable design of electrocatalytic materials with recognized interfacial structures will be a key challenge in the near future. The future challenges and prospects for the tailoring of electrocatalyst interactions at the interfacial level are illustrated in Fig. 16.

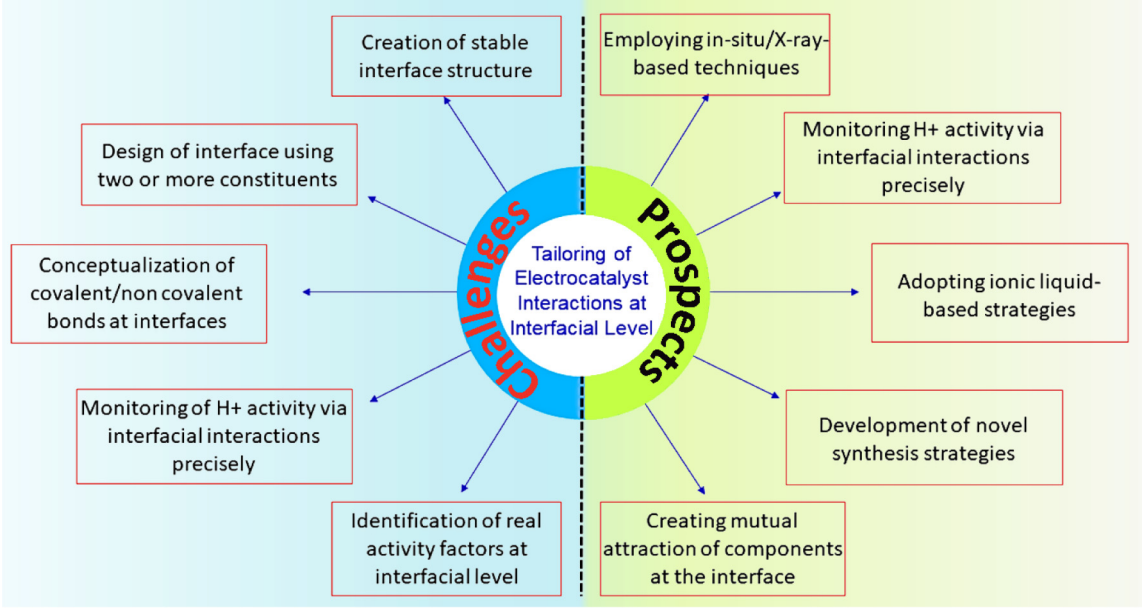

Fig. 16. Illustration of future challenges and prospects for the tailoring of electrocatalyst interactions at the interfacial level.

Declaration of Competing Interest

The authors declare that they have no known competing financial interests or personal relationships that could have appeared to influence the work reported in this paper.

Acknowledgments

This work was supported by the Research Fund for International Scientists (RFIS-Grant numbers: 52150410410) National Natural Science Foundation of China.

References

[1] Y. Yang, M. Luo, W. Zhang, Y. Sun, X. Chen, S. Guo, Chem 4 (9) (2018) 2054–2083.
[2] J.M. Mayer, Annu. Rev. Phys. Chem. 55 (2004) 363–390.
[3] I.C. Gerber, P. Serp, Chem. Rev. 120 (2019) 1250–1349.
[4] H. Xu, H. Shang, C. Wang, Y. Du, Coord. Chem. Rev. 418 (2020) 213374.
[5] P. Wang, H. Yang, Y. Xu, X. Huang, J. Wang, M. Zhong, T. Cheng, Q. Shao, ACS Nano 15 (2020) 1039–1047.
[6] I.E. Stephens, A.S. Bondarenko, U. Grønbjerg, J. Rossmeisl, I. Chorkendorff, Energy Environ. Sci. 5 (2012) 6744–6762.
[7] A.S. Arico, P. Bruce, B. Scrosati, J.M. Tarascon, W.V. Schalkwijk, Nat. Mater 4 (5) (2005) 366.
[8] W. Xu, Y. Bai, Y. Yin, Adv. Mater. 30 (2018) 1802091.
[9] B.E. Hayden, Acc. Chem. Res. 46 (2013) 1858–1866.
[10] C. Hu, Y. Lin, J.W. Connell, H.M. Cheng, Y. Gogotsi, M.M. Titirici, L. Dai, Adv. Mater. 31 (2019) 1806128.
[11] J. Lai, B. Huang, Y. Tang, F. Lin, P. Zhou, X. Chen, Y. Sun, F. Lv, S. Guo, Chem 4 (2018) 1153–1166.
[12] C. Yuan, H.B. Wu, Y. Xie, X.W. Lou, Angew. Chem. 53 (2014) 1488–1504.
[13] M.T. Koper, Chem. Sci. 4 (2013) 2710–2723.
[14] H. Li, C. Chen, D. Yan, Y. Wang, R. Chen, Y. Zou, S. Wang, J. Mater. Chem. A 7 (2019) 23432–23450.
[15] J. Huang, Y. Su, Y. Zhang, W. Wu, C. Wu, Y. Sun, R. Lu, G. Zou, Y. Li, J. Xiong, J. Mater. Chem. A 6 (2018) 9467–9472.
[16] J. Zhang, T. Wang, D. Pohl, B. Rellinghaus, R. Dong, S. Liu, X. Zhuang, X. Feng, Angew. Chem. 128 (2016) 6814–6819.
[17] X. Xu, C. Liu, Z. Sun, T. Cao, Z. Zhang, E. Wang, Z. Liu, K. Liu, Chem. Soc. Rev. 47 (2018) 3059–3099.
[18] Y.P. Zhu, C. Guo, Y. Zheng, S.-Z. Qiao, Acc. Chem. Res. 50 (2017) 915–923.
[19] P.F. Liu, X. Li, S. Yang, M.Y. Zu, P. Liu, B. Zhang, L.R. Zheng, H. Zhao, H.G. Yang, ACS Energy Lett. 2 (2017) 2257–2263.
[20] G. Chen, Y. Zhao, G. Fu, P.N. Duchesne, L. Gu, Y. Zheng, X. Weng, M. Chen, P. Zhang, C.-W. Pao, Science 344 (2014) 495–499.
[21] H. Wang, Y.-K. Tzeng, Y. Ji, Y. Li, J. Li, X. Zheng, A. Yang, Y. Liu, Y. Gong, L. Cai, Nat. Nanotechnol. 15 (2020) 131–137.
[22] C. Wang, S. Bai, Y. Xiong, Chinese J. Catal. 36 (2015) 1476–1493.
[23] Q. Shao, P. Wang, X. Huang, Adv. Funct. Mater. 29 (2019) 1806419.
[24] A. Khan, C.A. Gunawan, C. Zhao, Engineering ACS Sustain. Chem. Eng. 5 (2017) 3698–3715.
[25] Y. Zhang, Y. Lin, T. Duan, L. Song, Mater. Today 46 (2021) 115–134.
[26] A. Kumar, Y. Zhang, W. Liu, X. Sun, Coord. Chem. Rev. 402 (2020) 213047.
[27] A. Kumar, S. Ibraheem, T.A. Nguyen, R.K. Gupta, T. Maiyalagan, G. Yasin, Coord. Chem. Rev. 446 (2021) 214122.
[28] M. Melchionna, P. Fornasiero, M. Prato, Adv. Mater. 31 (2019) 1802920.
[29] A. Kumar, V.K. Vashistha, D.K. Das, S. Ibraheem, G. Yasin, R. Iqbal, T.A. Nguyen, R.K. Gupta, M.R. Islam, Fuel 304 (2021) 121420.
[30] Z.W. Seh, J. Kibsgaard, C.F. Dickens, I. Chorkendorff, J.K. Nørskov, T.F. Jaramillo, Science 355 (2017).
[31] S.C. Perry, D. Pangotra, L. Vieira, L.-I. Csepei, V. Sieber, L. Wang, C.P. de León, F. C. Walsh, Nano Res. 3 (2019) 442–458.
[32] H. Yi, M. Yan, D. Huang, G. Zeng, C. Lai, M. Li, X. Huo, L. Qin, S. Liu, X. Liu, Appl. Catal. B 250 (2019) 52–62.
[33] Z.W. Seh, J. Kibsgaard, C.F. Dickens, I. Chorkendorff, J.K. Nørskov, T.F. Jaramillo, Science 355 (2017) 4998.
[34] F. Calle-Vallejo, D. Loffreda, M.T. Koper, P. Sautet, J. Phys. Chem. Lett. 7 (2015) 403–410.
[35] J. Greeley, Annu. Rev. Chem. Biomol. Eng. 7 (2016) 605–635.
[36] M.M. Montemore, J.W. Medlin, J. Am. Chem. Soc. 136 (2014) 9272–9275.
[37] R. Christensen, H.A. Hansen, C.F. Dickens, J.K. Nørskov, T. Vegge, J. Phys. Chem. C 120 (2016) 24910–24916.
[38] I.C. Man, H.Y. Su, F. Calle-Vallejo, H.A. Hansen, J.I. Martínez, N.G. Inoglu, J. Kitchin, T.F. Jaramillo, J.K. Nørskov, J. Rossmeisl, ChemCatChem 3 (2011) 1159–1165.
[39] B. Hammer, J.K. Norskov, Nature 376 (1995) 238–240.
[40] A. Grimaud, K.J. May, C.E. Carlton, Y.-L. Lee, M. Risch, W.T. Hong, J. Zhou, Y. Shao-Horn, Nat. Commun. 4 (2013) 1–7.
[41] J. Suntivich, K.J. May, H.A. Gasteiger, J.B. Goodenough, Y. Shao-Horn, Science 334 (2011) 1383–1385.
[42] Y. Lee, J. Suntivich, K.J. May, E.E. Perry, Y. Shao-Horn, J. Phys. Chem. Lett. 3 (2012) 399–404.
[43] X. Ma, H. Xin, Phys. Rev. Lett. 118 (2017) 036101.
[44] W.T. Hong, K.A. Stoerzinger, Y.-L. Lee, L. Giordano, A. Grimaud, A.M. Johnson, J. Hwang, E.J. Crumlin, W. Yang, Y.J.E. Shao-Horn, E. Science 10 (2017) 2190–2200.
[45] W.T. Hong, M. Risch, K.A. Stoerzinger, A. Grimaud, J. Suntivich, Y.J.E. Shao-Horn, E. Science 8 (2015) 1404–1427.
[46] R. Chattot, O. Le Bacq, V. Beermann, S. Kühl, J. Herranz, S. Henning, L. Kühn, T. Asset, L. Guétaz, G. Renou, Nat. Mater. 17 (2018) 827–833.
[47] O. Diaz-Morales, D. Ferrus-Suspedra, M.T. Koper, Chem. Sci. 7 (2016) 2639–2645.
[48] C. Chen, Y. Kang, Z. Huo, Z. Zhu, W. Huang, H.L. Xin, J.D. Snyder, D. Li, J.A. Herron, M. Mavrikakis, Science 343 (2014) 1339–1343.
[49] J. Zhang, Q. Zhang, X. Feng, Adv. Mater. 31 (2019) 1808167.
[50] H. Qiao, H. Liu, Z. Huang, Q. Ma, S. Luo, J. Li, Y. Liu, J. Zhong, X.M. Qi, Adv. Energy Mater. 10 (2020) 2002424.
[51] Z. Zhang, P. Zhang, S. Yang, T. Zhang, M. Löffler, H. Shi, M.R. Lohe, X. Feng, Proc. Natl. Acad. Sci. 117 (2020) 13959–13966.
[52] X. Wang, R.K.M. Raghupathy, C.J. Querebillo, Z. Liao, D. Li, K. Lin, M. Hantusch, Z. Sofer, B. Li, E. Zschech, Adv. Mater. (2021) 2008752.
[53] Q. Jia, S. Ghoshal, J. Li, W. Liang, G. Meng, H. Che, S. Zhang, Z.-F. Ma, S.J. Mukerjee, J. Am. Chem. Soc. 139 (2017) 7893–7903.
[54] C. Reich, A. Kaiser, J. Irvine, Fuel Cells 1 (2001) 249–255.
[55] S. Tauster, S. Fung, R. Baker, J. Horsley, Science 211 (1981) 1121–1125.
[56] B. Gates, Chem. Rev. 95 (1995) 511–522.
[57] M. Luo, S. Guo, Nat. Rev. Mater. 2 (2017) 1–13.
[58] L. Bu, S. Guo, X. Zhang, X. Shen, D. Su, G. Lu, X. Zhu, J. Yao, J. Guo, X. Huang, Nat. Commun. 7 (2016) 1–10.
[59] J. Wu, L. Qi, H. You, A. Gross, J. Li, H. Yang, J. Am. Chem. Soc. 134 (2012) 11880–11881.
[60] Y. Xie, Z.-W. Wang, T.-Y. Zhu, D.-J. Shu, Z.-F. Hou, K. Terakura, Carbon 139 (2018) 129–136.
[61] J.K. Nørskov, F. Abild-Pedersen, F. Studt, T. Bligaard, Proc. Natl. Acad. Sci. 108 (2011) 937–943.
[62] M. Shao, Q. Chang, J.-P. Dodelet, R. Chenitz, Chem. Rev. 116 (2016) 3594–3657.
[63] C. Xu, L. Wang, Z. Liu, L. Chen, J. Guo, N. Kang, X.-L. Ma, H.-M. Cheng, W. Ren, Nat. Mater. 14 (2015) 1135–1141.
[64] M. Luo, Y. Sun, L. Wang, S. Guo, Adv. Energy Mater. 7 (2017) 1602073.
[65] W. Zhu, H. Yuan, F. Liao, Y. Shen, H. Shi, Y. Shi, L. Xu, M. Ma, M. Shao, Chem. Eng. J. 389 (2020) 124240.
[66] A. Khorshidi, J. Violet, J. Hashemi, A.A. Peterson, Nat. Catal. 1 (2018) 263–268.
[67] J. Liu, J. Ma, Z. Zhang, Y. Qin, Y.-J. Wang, Y. Wang, R. Tan, X. Duan, T.Z. Tian, C. H. Zhang, Mater. Today Phys. 4 (2021) 022004.
[68] J. Liang, Z. Zhao, N. Li, X. Wang, S. Li, X. Liu, T. Wang, G. Lu, D. Wang, B. Hwang, Adv. Energy Mater. 10 (2020) 2000179.
[69] T. Wang, Y. Zhang, B. Huang, B. Cai, R.R. Rao, L. Giordano, S.-G. Sun, Y. Shao-Horn, Nat. Catal. 4 (2021) 753–762.
[70] E.M. Higgins, J.A. Sherwood, A.G. Lindsay, J. Armstrong, R.S. Massey, R.W. Alder, A.C. O'Donoghue, ChemComm 47 (2011) 1559–1561.
[71] K. Kaupmees, A. Trummal, I. Leito, Croat. Chem. Acta 87 (2014) 385–395.
[72] Y. Otake, H. Nakamura, S. Fuse, Angew. Chem. 57 (2018) 11389–11393.
[73] G.-R. Zhang, T. Wolker, D.J. Sandbeck, M. Munoz, K.J. Mayrhofer, S. Cherevko, B. Etzold, ACS Catal. 8 (2018) 8244–8254.
[74] S. Favero, I.E. Stephens, M.M. Titirici, S. Research, Adv. Sustain. Syst. 2 (2021) 2000062.
[75] J. Snyder, K. Livi, J. Erlebacher, Adv. Funct. Mater. 23 (2013) 5494–5501.
[76] J. He, C. Yang, X. Yang, L. Liu, J. Li, Q. Liu, L. Peng, X. Liu, M. Qu, Appl. Surf. Sci. 532 (2020) 147357.
[77] M. Nakamura, Y. Nakajima, N. Hoshi, H. Tajiri, O. Sakata, ChemPhysChem 14 (2013) 2426–2431.
[78] D. Strmcnik, K. Kodama, D. van der Vliet, J. Greeley, V.R. Stamenkovic, N. Marković, Nat. Chem. 1 (2009) 466–472.
[79] T. Kumeda, H. Tajiri, O. Sakata, N. Hoshi, M. Nakamura, Nat. Commun. 9 (2018) 1–7.
[80] S.J. Kim, J.Y. Koo, T. Mun, M. Choi, W. Lee, J. Mater. Chem. A 8 (2020) 23313–23322.
[81] Q. Xu, L. Zhao, R. Yuan, Y. Chen, Z. Xue, J. Zhang, X. Qiu, J. Qu, Colloids Surf. A Physicochem. Eng. Asp. 629 (2021) 127435.
[82] L. Zhao, Q. Xu, Z. Shao, Y. Chen, Z. Xue, H. Li, J. Zhang, ACS Appl. Mater. Interfaces 12 (2020) 45976–45986.
[83] Q. Xu, L. Zhao, Y. Ma, R. Yuan, M. Liu, Z. Xue, H. Li, J. Zhang, X. Qiu, J. Colloid Interface Sci. 597 (2021) 269–277.
[84] S.J. Kim, J. Baek, M. Choi, J. Lee, W. Lee, J. Power Sources 509 (2021) 230351.
[85] X.Y. Zhou, C. Xu, P.P. Guo, W.L. Sun, P.J. Wei, J.G. Liu, Chem. Eur. J. 27 (2021) 9898–9904.
[86] J.H. Shim, J.S. Park, T.P. Holme, K. Crabb, W. Lee, Y.B. Kim, X. Tian, T.M. Gür, F. B. Prinz, Acta Mater. 60 (2012) 1–7.
[87] H. Kang, W. Wang, J. Shi, Z. Xu, H. Lv, X. Qian, L. Liu, M. Jing, F. Li, J. Niu, Appl. Surf. Sci. 465 (2019) 1103–1106.
[88] W. Jiang, H. Wang, Z. Xu, N. Li, C. Chen, C. Li, J. Li, H. Lv, L. Kuang, X. Tian, Chem. Eng. J. 335 (2018) 954–969.
[89] H. Wang, N. Li, W. Wang, J. Shi, Z. Xu, L. Liu, Y. Hu, M. Jing, L. Liu, X. Zhang, Chem. Eng. J. 360 (2019) 1241–1246.

[90] H. Wang, T. Sun, L. Chang, P. Nie, X. Zhang, C. Zhao, X. Xue, Electrochim. Acta 303 (2019) 110–117.
[91] H. Wang, X. Yuan, H. Wang, X. Chen, Z. Wu, L. Jiang, W. Xiong, G. Zeng, Appl. Catal. B 193 (2016) 36–46.
[92] H. Huang, S. Yang, R. Vajtai, X. Wang, P.M. Ajayan, Adv. Mater. 26 (2014) 5160–5165.
[93] X. Shi, W. Wang, X. Miao, F. Tian, Z. Xu, N. Li, M. Jing, ACS Appl. Mater. Interfaces 12 (2020) 46095–46106.
[94] Y.-C. Lu, Z. Xu, H.A. Gasteiger, S. Chen, K. Hamad-Schifferli, Y. Shao-Horn, J. Am. Chem. Soc. 132 (2010) 12170–12171.
[95] A. Fortunelli, W.A. Goddard, Y. Sha, T.H. Yu, L. Sementa, G. Barcaro, O. Andreussi, Angew. Chem. 126 (2014) 6787–6790.
[96] F. Calle-Vallejo, A. Krabbe, J.M. García-Lastra, Chem. Sci. 8 (2017) 124–130.
[97] N. Govindarajan, J.M. García-Lastra, E.J. Meijer, F. Calle-Vallejo, Curr. Opin. Electrochem. 8 (2018) 110–117.
[98] Q. Ma, H. Jin, J. Zhu, Z. Li, H. Xu, B. Liu, Z. Zhang, J. Ma, S. Mu, Adv. Sci. 8 (2021) 2102209.
[99] I.S. Amiinu, X. Liu, Z. Pu, W. Li, Q. Li, J. Zhang, H. Tang, H. Zhang, S. Mu, Adv. Funct. Mater. 28 (2018) 1704638.
[100] H. Shang, Z. Jiang, D. Zhou, J. Pei, Y. Wang, J. Dong, X. Zheng, J. Zhang, W. Chen, Chem. Sci. 11 (23) (2020) 5994–5999.
[101] Z. Jiang, W. Sun, H. Shang, W. Chen, T. Sun, H. Li, J. Dong, J. Zhou, Z. Li, Y. Wang, Energy Environ. Sci. 12 (2019) 3508–3514.
[102] Z. Zhang, H. Jin, J. Zhu, W. Li, C. Zhang, J. Zhao, F. Luo, Z. Sun, S. Mu, Carbon 161 (2020) 502–509.
[103] D. Chen, J. Zhu, X. Mu, R. Cheng, W. Li, S. Liu, Z. Pu, C. Lin, S. Mu, Appl. Catal. B 268 (2020) 118729.
[104] I.S. Amiinu, Z. Pu, X. Liu, K.A. Owusu, H.G.R. Monestel, F.O. Boakye, H. Zhang, S. Mu, Adv. Funct. Mater. 27 (2017) 1702300.
[105] H. Jin, H. Zhou, P. Ji, C. Zhang, J. Luo, W. Zeng, C. Hu, D. He, S. Mu, Nano Res. 13 (2020) 818–823.
[106] Z. Xue, X. Li, Q. Liu, M. Cai, K. Liu, M. Liu, Z. Ke, X. Liu, G. Li, Adv. Mater. 31 (2019) 1900430.
[107] Z. Xue, K. Liu, Q. Liu, Y. Li, M. Li, C.-Y. Su, N. Ogiwara, H. Kobayashi, H. Kitagawa, M. Liu, Nat. Commun. 10 (2019) 1–8.
[108] Z. Wang, H. Jin, T. Meng, K. Liao, W. Meng, J. Yang, D. He, Y. Xiong, S. Mu, Adv. Funct. Mater. 28 (2018) 1802596.
[109] W. Li, Y. Xiong, Z. Wang, M. Bao, J. Liu, D. He, S. Mu, Appl. Catal. B 231 (2018) 277–282.
[110] M. Jahan, Q. Bao, K.P. Loh, J. Am. Chem. Soc. 134 (2012) 6707–6713.
[111] J.P. Collman, L. Fu, P.C. Herrmann, X. Zhang, Science 275 (1997) 949–951.
[112] J.P. Collman, N.K. Devaraj, R.A. Decréau, Y. Yang, Y.-L. Yan, W. Ebina, T.A. Eberspacher, C.E. Chidsey, Science 315 (2007) 1565–1568.
[113] C.J. Chang, L.L. Chng, D.G.J. Nocera, J. Am. Chem. Soc. 125 (2003) 1866–1876.
[114] Z. Yu, C. Liu, Y. Deng, M. Li, F. She, L. Lai, Y. Chen, L. Wei, Chinese J. Catal. 43 (2022) 1238–1246.
[115] Y. Ma, J. Li, X. Liao, W. Luo, W. Huang, J. Meng, Q. Chen, S. Xi, R. Yu, Y. Zhao, Adv. Funct. Mater. 30 (2020) 2005000.
[116] Y. Li, S. Wu, B. Su, Chem. Eur. J. 18 (2012) 7372–7376.
[117] Y. Li, B. Jia, Y. Fan, K. Zhu, G. Li, C.Y. Su, Adv. Energy Mater. 8 (2018) 1702048.
[118] L. Xie, X. Li, B. Wang, J. Meng, H. Lei, W. Zhang, R. Cao, Angew. Chem. Int. Ed. 58 (52) (2019) 18883–18887.
[119] A. Kumar, G. Yasin, M. Tabish, D.K. Das, S. Ajmal, A.K. Nadda, G. Zhang, T. Maiyalagan, A. Saad, R.K. Gupta, M.M. Makhlouf, Chem. Eng. J. (2022) 136784.
[120] M.P. Oyarzún, N. Silva, D. Cortés-Arriagada, J. Silva, I.O. Ponce, M. Flores, K. Tammeveski, D. Bélanger, A. Zitolo, F. Jaouen, J.H. Zagal, Electrochim. Acta 398 (2021) 139263.
[121] J. Meng, H. Lei, X. Li, J. Qi, W. Zhang, R. Cao, ACS Catal. 9 (5) (2019) 4551–4560.
[122] V.S. Thimmakondu, M. Bouvet, M. Bertotti, K. Araki, Chem. Commun. 55 (84) (2019) 12719–12720.
[123] I. Hijazi, T. Bourgeteau, R. Cornut, A. Morozan, A. Filoramo, J. Leroy, V. Derycke, B. Jousselme, S. Campidelli, J. Am. Chem. Soc. 136 (17) (2014) 6348–6354.
[124] R. Cao, R. Thapa, H. Kim, X. Xu, M. Gyu Kim, Q. Li, N. Park, M. Liu, J. Cho, Nat. Commun. 4 (1) (2013) 1–7.
[125] J. Riquelme, K. Neira, J.F. Marco, P. Hermosilla-Ibáñez, W. Orellana, J.H. Zagal, F. Tasca, Electrochim. Acta 265 (2018) 547–555.
[126] J. Huang, Q. Lu, X. Ma, X. Yang, J. Mater. Chem. A 6 (38) (2018) 18488–18497.
[127] J. Guo, X. Yan, Q. Liu, Q. Li, X. Xu, L. Kang, Z. Cao, G. Chai, J. Chen, Y. Wang, J. Yao, Nano Energy 46 (2018) 347–355.
[128] X.Y. Zhou, C. Xu, P.P. Guo, W.L. Sun, P.J. Wei, J.G. Liu, Chem. Eur. J. 27 (38) (2021) 9898–9904.
[129] Z. Liang, H. Guo, G. Zhou, K. Guo, B. Wang, H. Lei, W. Zhang, H. Zheng, U.P. Apfel, R. Cao, Angew. Chem. Int. Ed. 60 (15) (2021) 8472–8476.
[130] S. Ibraheem, G. Yasin, A. Kumar, M.A. Mushtaq, S. Ibrahim, R. Iqbal, M. Tabish, S. Ali, A. Saad, Appl. Catal. B 304 (2022) 120987.
[131] G. Yasin, S. Ibrahim, S. Ibraheem, S. Ali, R. Iqbal, A. Kumar, M. Tabish, Y. Slimani, T. A. Nguyen, H. Xu, W. Zhao, J. Mater. Chem. A 9 (2021) 18222–18230.
[132] G. Yasin, S. Ibraheem, S. Ali, M. Arif, S. Ibrahim, R. Iqbal, A. Kumar, M. Tabish, M. A. Mushtaq, A. Saad, H. Xu, W. Zhao, Mater. Today Chem. 23 (2022) 100634.
[133] G. Yasin, M. Arif, J. Ma, S. Ibraheem, D. Yu, L. Zhang, D. Liu, L. Dai, Inorg. Chem. Front. 9 (2022) 1058–1069.
[134] G. Yasin, M. Arif, T. Mehtab, M. Shakeel, M. A. Mushtaq, A. Kumar, T. A. Nguyen, Y. Slimani, M. T. Nazir, H. Song, Inorg. Chem. Front. 7 (2020) 402–410.
[135] D. Yu, A. Kumar, T. A. Nguyen, M. T. Nazir, G. Yasin, ACS Sustainable Chem. Eng. 8 (2020) 13769–13776.
[136] G. Yasin, M. Arif, T. Mehtab, X. Lu, D. Yu, N. Muhammad, M. T. Nazir, H. Song, Energy Storage Mater. 25 (2020) 644–678.
[137] T. Mehtab, G. Yasin, M. Arif, M. Shakeel, R. M. Korai, M. Nadeem, N. Muhammad, X. Lu, J. Energy Storage 21 (2019) 632–646.
[138] S. Ajmal, Y. Yang, K. Li, M. A. Tahir, Y. Liu, T. Wang, A. Bacha, Yi. Feng, Y. Deng, L. Zhang, J. Phys. Chem. C 18 (2019) 11555–11563.
[139] R. Iqbal, G. Yasin, M. Hamza, S. Ibraheem, B. Ullah, A. Saleem, S. Ali, S. Hussain, T. A. Nguyen, Y. Slimani, R. Pathak, Coord. Chem. Rev. 447 (2021) 214152.
[140] M.A. Mushtaq, M. Arif, X. Fang, G. Yasin, W. e, M. Basharat, B. Zhou, S. Yang, S. Ji, D. Yan, J. Mater. Chem. A 9 (2021) 2742–2753.
[141] S. Ibraheem, S. Chen, L. Peng, J. Li, L. Li, Q. Liao, M. Shao, Z. Wei, Appl. Catal. B 265 (2020) 118569.

Ghulam Yasin received his Bachelor of Engineering in Metallurgy and Materials from the Institute of Advanced Materials, Bahauddin Zakariya University, Multan, Pakistan. He did his Master and Ph.D. in Materials Science and Engineering from the College of Materials Science and Engineering, Beijing University of Chemical Technology, Beijing, China. He was working as a Research Assistant at the Institute of Nuclear & New Energy Technology, Tsinghua University, Beijing, China in 2020. Currently, he is working as a Research Fellow at the Institute for Advanced Study, and College of Physics and Optoelectronic Engineering, Shenzhen University, Shenzhen, Guangdong, China. Dr. Yasin has over 120 publications in well-reputed peer-reviewed journals. He is the author of several book chapters and Editor of 20 Elsevier books in the Micro & Nano Technologies Series, as well as CRC Press Engineering. He has been awarded various national and international honors and awards. Dr. Yasin has ranked among the world's top 2% scientists (by Elsevier BV, and Standford University, USA). Dr. Yasin is serving as Associate Editor, Section Editor, Guest Editor, and editorial board member for several journals. His research focuses on the design and development of advanced functional nanomaterials for energy conversion and storage hybrid devices/technologies, as well as nanostructures and nanomaterials for various functional applications.

Sehrish Ibrahim received her Master of Science from the University of Education, Lahore, Pakistan. She is currently a Ph.D. student at the Beijing University of Chemical Technology, Beijing, China. She has published several research articles in peer-reviewed journals and also authored many book chapters in the area of Micro and Nanotechnology. Her research involves advanced nanomaterials and nanosystems for biomedical and energy-related applications.

Saira Ajmal received her Ph.D. in 2020 from the Fudan University, Shanghai, China with a specialization in Environmental Chemistry. Dr. Saira is currently working as a Postdoctoral Research Fellow at the Institute for Advanced Study, and College of Physics and Optoelectronic Engineering, Shenzhen University, Shenzhen, Guangdong, China. She has published more than 30 articles in peer-reviewed journals and various Book Chapters. She has won the international student Ph.D. Fellowship from the world's top 50, the Fudan University. Her research focus is on advanced materials for electrocatalysis and photoelectrocatalysis.

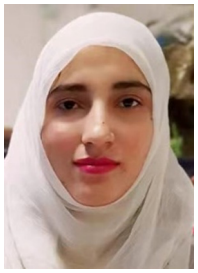

Shumaila Ibraheem received her Ph.D. in 2019 from the Chongqing University, Chongqing, China with a specialization in New Energy Materials. Dr. Shumaila is presently working as a Postdoctoral Researcher at the Institute for Advanced Study, Shenzhen University, Shenzhen, Guangdong, China. She has published more than 50 scientific contributions in the form of Research and Review articles in peer-reviewed prestigious journals, as well as Book Chapters. She has won several honors and awards, including the Outstanding International Graduate Student Award of Chongqing University and the Academic Progress Award from Chongqing University. Her research interests include nanostructures and nanomaterials for electrochemical energy conversion and storage devices, particularly oxygen reduction reactions, oxygen evolution reactions, hydrogen evolution reactions, water electrolyzers, fuel cells, supercapacitors, metal-air batteries, as well as metal-ion batteries.

Sajjad Ali received his Ph.D. in Materials Science and Engineering from the University of Chinese Academy of Science, China. He was working as a Postdoctoral Fellow at the Southern University of Science and Technology, Shenzhen, China from 2019 to 2022. Currently, he is working as a Research Fellow at Yangtze Delta Research Institute Huzhou, University of Electronic Science and Technology of China. Dr. Sajjad has over 50 publications in well-reputed peer-reviewed journals. His research interests focus on understanding the structure, electronic, magnetic, and catalytic properties of 1D, 2D, and 3D materials, including MOFs and COFs, for energy storage devices, CO_2 conversion to valuable products, electrochemical reactions, such as ORR, OER, HER, etc.

Anuj Kumar is an Assistant Professor at the GLA University, Mathura, India. His research focus is on molecular and M-N-C electrocatalysts for H_2, O_2, and CO_2 involving electrocatalysis, nanomaterials, nanocomposites, fuel cells, water electrolyzers, nanosensors, bio-inorganic chemistry, macrocyclic chemistry. He has published more than 60 articles in reputed peer-reviewed journals. He has also contributed more than 20 book chapters to Elsevier, Springer, CRC Press, and the Bentham Science book series. For outstanding contribution in his research field, He has been awarded the "Best Young Scientist Award 2021" from the Tamil Nadu Association of Intellectuals and Faculty (TAIF) and GRBS Educational Charitable Trust, India. "Young Researcher Award 2020", by Central Education Growth and Research (CEGR), India. He is serving as Section Editor, Guest editor, and editorial board member for various journals.